



## Aggregation of recount3 RNA-seq data improves inference of consensus and tissue-specific gene coexpression networks

Prashanthi Ravichandran, Princy Parsana, Rebecca Keener, et al.

*Genome Res.* published online July 17, 2025

Access the most recent version at doi:[10.1101/gr.280808.125](https://doi.org/10.1101/gr.280808.125)

---

<b>P&lt;P</b>	Published online July 17, 2025 in advance of the print journal.
<b>Accepted Manuscript</b>	Peer-reviewed and accepted for publication but not copyedited or typeset; accepted manuscript is likely to differ from the final, published version.
<b>Open Access</b>	Freely available online through the <i>Genome Research</i> Open Access option.
<b>Creative Commons License</b>	This manuscript is Open Access. This article, published in <i>Genome Research</i> , is available under a Creative Commons License (Attribution-NonCommercial 4.0 International license), as described at <a href="http://creativecommons.org/licenses/by-nc/4.0/">http://creativecommons.org/licenses/by-nc/4.0/</a> .
<b>Email Alerting Service</b>	Receive free email alerts when new articles cite this article - sign up in the box at the top right corner of the article or <a href="#">click here</a> .

---

---

Advance online articles have been peer reviewed and accepted for publication but have not yet appeared in the paper journal (edited, typeset versions may be posted when available prior to final publication). Advance online articles are citable and establish publication priority; they are indexed by PubMed from initial publication. Citations to Advance online articles must include the digital object identifier (DOIs) and date of initial publication.

---

To subscribe to *Genome Research* go to:  
<https://genome.cshlp.org/subscriptions>

---

Published by Cold Spring Harbor Laboratory Press

Running title: DATA AGGREGATION IMPROVES NETWORK INFERENCE

# 1 **Aggregation of recount3 RNA-seq data improves inference of**

## 2 **consensus and tissue-specific gene co-expression networks**

3 Prashanthi Ravichandran<sup>1</sup>, Princy Parsana<sup>2</sup>, Rebecca Keener<sup>1</sup>, Kasper D.

4 Hansen<sup>1,3,4</sup>, Alexis Battle<sup>\*1,2,4,5,6</sup>

5 1. Department of Biomedical Engineering, Johns Hopkins University, Baltimore, MD, USA

6 2. Department of Computer Science, Johns Hopkins University, Baltimore, MD, USA

7 3. Department of Biostatistics, Johns Hopkins School of Public Health, Baltimore, MD, USA

8 4. Department of Genetic Medicine, Johns Hopkins University, Baltimore, MD, USA

9 5. Malone Center for Engineering in Healthcare, Johns Hopkins University, Baltimore, MD, USA

10 6. Data Science and AI Institute, Johns Hopkins University, Baltimore, MD, USA

11 \* Corresponding author

12

13 Alexis Battle, PhD

14 [ajbattle@jhu.edu](mailto:ajbattle@jhu.edu)

15

## 16 **Keywords**

17 Gene co-expression networks (GCNs), Graphical lasso, recount3, Public RNA-seq data, SRA,

18 GTEx, TCGA, Data aggregation, Context-specificity, Complex trait heritability, s-LDSC.

## 19 Abstract

20 Gene co-expression networks (GCNs) describe relationships among genes that maintain  
21 cellular identity and homeostasis. However, typical RNA-seq experiments often lack sufficient  
22 sample sizes for reliable GCN inference. Recount3, a dataset with 316,443 processed human  
23 RNA-seq samples, provides an opportunity to improve network reconstruction. However, GCN  
24 inference from public data is challenged by confounders and inconsistent labeling. To address  
25 this, we developed a pipeline to annotate samples based on cell-type composition. By comparing  
26 aggregation strategies, we found that regressing confounders within studies and prioritizing  
27 larger studies optimized network reconstruction. We applied these findings to infer three  
28 consensus networks (universal, cancer, non-cancer) and 27 context-specific networks. Central  
29 genes in consensus networks were enriched for evolutionarily constrained genes and ubiquitous  
30 biological pathways, while context-specific central nodes included tissue-specific transcription  
31 factors. The increased statistical power from data aggregation facilitated the derivation of variant  
32 annotations from context-specific networks, which were significantly enriched for complex-trait  
33 heritability independent of overlap with baseline functional genomic annotations. While data  
34 aggregation led to strictly increasing held-out log-likelihood, we observed diminishing marginal  
35 improvements, suggesting that integrating complementary modalities, such as Hi-C and  
36 ChIP-seq, could further refine network reconstruction. Our approach outlines best practices for  
37 GCN inference and highlights both the strengths and limitations of data aggregation.

## 38 Introduction

39 Critical cellular processes including the maintenance of cellular identity, homeostasis,  
40 and the cellular response to external stimuli are orchestrated through complex transcriptional  
41 co-regulation of multiple genes (Hartwell et al. 1999; Hasty, McMillen, and Collins 2002; Oltvai

42 and Barabási 2002; Alon 2003). Gene Co-expression Networks (GCNs) are a commonly used  
43 framework to describe gene-gene relationships and are comprised of nodes that represent genes  
44 and edges linking co-expressed genes (Stuart et al. 2003). A comprehensive catalogue of gene  
45 co-expression relationships has the potential to characterize genes with unknown functions  
46 (Schlitt et al. 2003), identify regulatory genes (Narang et al. 2015), determine changes in  
47 regulatory mechanisms that are key to cellular identity (Wang, Choi, and Roeder 2021), and  
48 prioritize genes that drive phenotypic variability (van Dam et al. 2017).

49       Despite the utility of GCNs in understanding biological systems, network inference is  
50 still a challenging problem and suffers from both false positive and negative edges (Diaz and  
51 Stumpf 2022). In particular, the typical sample size of most RNA-seq studies is orders of  
52 magnitude smaller than the number of gene pairs over which regulatory relationships are  
53 inferred, making network inference an underdetermined problem. Additionally, factors such as  
54 the stochastic nature of gene expression, experimental noise, missing data, and unobserved  
55 technical confounders make it difficult to avoid false positives or negatives.

56       Since the number of possible gene-gene interactions scales with the square of the number  
57 of genes examined, a potential solution to increase statistical power by reducing network  
58 complexity has been to utilize methods such as WGCNA that infer modules or groups of  
59 co-expressed genes that are regulated by one or more transcription factors rather than individual  
60 gene interactions (Segal et al. 2003). While this approach has been successful at decreasing the  
61 number of hypotheses tested, and thereby increasing statistical power (Wolf et al. 2014), it does  
62 not identify detailed network structure or distinguish between direct and indirect gene  
63 interactions. In contrast, network inference by graphical lasso (Friedman, Hastie, and Tibshirani  
64 2008; Hastie, Tibshirani, and Friedman 2013) results in the identification of pairwise edges

65 reflecting direct effects, such that the absence of an edge implies the conditional independence of  
66 the genes when all other genes are observed. Further, the formulation of graphical lasso enables  
67 flexible penalization based on the number of edges found in the network which aids in the  
68 identification of a network structure that improves the discovery of true gene-gene interactions  
69 while reducing false positives (Huang, Lu, and Hsiao 2020). Here, we focus on improving the  
70 statistical power of network inference by significantly increasing the number of samples used in  
71 network inference, leveraging large-scale publicly available and uniformly processed RNA-seq  
72 data from recount3 (Wilks et al. 2021) which includes human RNA-seq samples from GTEx  
73 (The GTEx Consortium 2020), TCGA (Tomczak, Czerwińska, and Wiznerowicz 2015), and  
74 SRA (Katz et al. 2022; Kodama et al. 2012).

75       Public RNA-seq data resources such as recount3 offer an unprecedented opportunity to  
76 improve GCN inference, but also present major challenges due to heterogeneity in sample  
77 preparation, sequencing protocols, missing or inconsistent metadata, and variation in biological  
78 and technical factors across studies. To address these challenges, we set out to develop a data  
79 pre-processing pipeline that can identify and exclude outliers, harmonize expression  
80 measurements across studies, and group samples into biologically meaningful contexts  
81 appropriate for network reconstruction.

82       While statistical methods for confounder correction have been widely applied within  
83 individual studies (Parsana et al. 2019), it remains unclear how best to account for confounding  
84 and integrate data across multiple studies in a way that preserves true biological signal and  
85 enhances the quality of network inference. This motivated us to systematically evaluate  
86 strategies for confounder adjustment and data aggregation across studies. Finally, to assess the  
87 utility of these networks for downstream biological discovery, we examine the relevance of

88 inferred network features, such as node centrality, to known regulatory roles and their  
89 enrichment for complex trait heritability using stratified LD score regression (S-LDSC; Finucane  
90 et al., 2015). In summary, our study seeks to provide a carefully annotated RNA-seq data set,  
91 outline best practices for GCN inference by leveraging publicly available RNA-seq data, and a  
92 set of consensus and context-specific networks that will aid the scientific community in  
93 achieving the full potential of GCN inference in biomedical research.

## 94 **Results**

95 Manual annotation and clustering of RNA-seq data from recount3 identified 27  
96 unique tissue contexts

97 We downloaded uniformly processed RNA-seq samples from humans using the recount3  
98 R package (Wilks et al. 2021) comprised of experiments from three data sources, The Sequence  
99 Read Archive (SRA) (Kodama et al. 2012; Katz et al. 2022), Genotype-tissue Expression (GTEx  
100 version 8) (The GTEx Consortium 2020), and The Cancer Genome Atlas (TCGA) (Tomczak,  
101 Czerwińska, and Wiznerowicz 2015) and selected 1,747 projects that included 30 or more  
102 samples each. Following quality control (**Methods**), 95,280 human bulk-RNA sequencing  
103 samples remained from 50 GTEx tissues (18,828 samples), 33 TCGA cancer types (11,091  
104 samples), and 884 SRA studies (65,361 samples) (**Fig. 1 A**). The number of genes present  
105 following data pre-processing varied by study and is summarized in **Supplemental Fig. S1**. The  
106 aggregated data includes samples from a wide array of tissues, cell types, and diseases. While  
107 GTEx and TCGA studies included metadata specifying the tissue of origin and disease status for  
108 all samples, SRA studies had inconsistent nomenclature. Therefore, to obtain reliable labels for  
109 SRA samples, we manually parsed sample descriptions to obtain sample characteristics  
110 corresponding to tissue type and disease status for 65,361 SRA samples (**Methods**). Based on

111 curated annotations, 93.5% of TCGA samples and 30.4% of SRA samples were cancer. In  
112 contrast, all GTEx samples were non-cancer, as expected (**Fig. 1 B**). Tissue labels with the  
113 greatest number of samples across all three data sources included blood, central nervous system,  
114 breast, skin, and lung (**Fig. 1 C**). SRA included 224 distinct tissue labels derived from manual  
115 annotation that was not observed in GTEx or TCGA, and reflected a wide range of disease states  
116 including Type I Diabetes, Alzheimer's disease, bipolar disorder, arthritis, cancer, and infectious  
117 conditions (**Fig. 1 D**). We grouped SRA samples based on their study accession IDs, GTEx  
118 samples by tissue, and TCGA samples by cancer code (**Methods**). To simplify terminology, we  
119 defined each group of samples from a data source as a single study. To leverage the extensive  
120 biological diversity in the data, we inferred two broad types of networks: consensus and tissue  
121 context-specific (context-specific). Our universal consensus network included all samples,  
122 regardless of tissue or disease. Our non-cancer consensus network included healthy samples and  
123 samples with disease status other than cancer. Finally, our cancer consensus network solely  
124 included cancerous samples. We restricted our context-specific networks to non-cancerous  
125 samples grouped by tissue context. We did not examine differential coregulation resulting from  
126 non-cancer disease, and regressed these effects from gene expression. Thus, by including SRA,  
127 recount3 provides an unprecedented opportunity to examine unique contexts that were not  
128 previously studied in GTEx and TCGA.

129        Across the three data sources, SRA, GTEx, and TCGA, we obtained 266 unique  
130 manually annotated tissue labels with a median sample size of 31 which was much lower than  
131 the number of protein-coding genes. Therefore, we used a study-pooling strategy based on  
132 related tissue contexts to increase power (**Methods**). Specifically, in this work, we define a tissue  
133 context as a group of samples with similar cell-type composition, which we infer

134 computationally. Mapping manual annotations to tissue contexts (**Supplemental Table S1**)  
135 generated 48 tissue contexts across 63,193 non-cancerous samples for context-specific network  
136 analysis. In each context, to ensure that a tissue context represented samples with similar  
137 cell-type composition as estimated by xCell (Aran, Hu, and Butte 2017) deconvolution, we  
138 learned a joint lower-dimensional t-SNE embedding using cell-type deconvolution scores, and  
139 for 25 contexts with more than 500 samples before outlier exclusion, we detected and excluded  
140 outliers (**Supplemental Fig. S2**). For the immune context, we observed that samples displayed  
141 extensive heterogeneity in cell-type composition. Thus we further separated this group into  
142 B cells, PBMCs/ T cells, and myeloid cells (**Supplemental Fig. S3**). Finally, we examined the  
143 differences in the empirical covariance estimates obtained when we considered alternate  
144 thresholds to exclude outliers, and found that while we observed minor differences across  
145 covariance estimates obtained by varying the exclusion criterion, these differences were much  
146 smaller than the differences in empirical covariance matrices between unrelated contexts, and  
147 hence selected samples that were found to be outliers by fewer than two methods, to ensure we  
148 considered the maximum possible number of samples for each context, while minimizing  
149 outliers that may truly reflect different contexts. (**Supplemental Fig. S4**).

150 In total, we obtained 27 contexts including 7 tissue contexts that were not present in  
151 GTEx: airway, eye, human embryonic stem cells, induced pluripotent stem cells, multipotent  
152 cells, myeloid cells, and PBMCs / T cells (**Fig. 1 E**). The number of samples present in each  
153 tissue context following outlier exclusion varied from 8,797 (Blood) to 485 (Multipotent cells)  
154 (**Fig. 1 F**). Of the tissue categories present in GTEx we were able to significantly increase the  
155 number of samples for several tissue contexts including blood, central nervous system, skin, and  
156 liver (**Fig. 1 F**). These harmonized samples have increased context resolution, i.e. include novel

157 contexts which were not examined in GTEx, and increased sample size which can be used to  
158 improve the inference of consensus and context-specific networks.

### 159 Data aggregation improves the inference of consensus and context-specific GCNs

160 The median study-specific sample size across the three data sources was 44 for SRA, 309  
161 for TCGA, and 285 for GTEx. Further, 766 of 884 SRA studies had a sample size lesser than  
162 100. PC-based data correction has been used within a single study to reduce potential false  
163 positive gene regulatory associations (Leek et al. 2012; Parsana et al. 2019), but best practices  
164 for applying PC-based data correction in the context of aggregating multiple studies to infer  
165 GCNs have not been fully examined. First, we sought to determine whether data correction  
166 should be performed jointly across all samples, across samples belonging to a specific tissue  
167 context and multiple studies, or across samples from a specific tissue context and a specific  
168 study. We observed that PCs recapitulate different sample characteristics depending on the level  
169 at which data aggregation is performed. PCs calculated across all samples were driven  
170 predominantly by tissue labels followed by technical confounders (e.g. study and data source)  
171 (**Supplemental Fig. S5 A-D, Supplemental Fig. S6 A**). PCs which were calculated across  
172 samples belonging to a single tissue context (blood) but multiple studies were predominantly  
173 driven by study and data source. Further, accounting for tissue heterogeneity enabled us to better  
174 model cancer status and disease annotations using PCs (**Supplemental Fig. S5 E-H,**  
175 **Supplemental Fig. S6 B**). Finally, when we limited samples to a specific tissue context and a  
176 specific study (GTEx-skeletal muscle), we found that the top PCs were significantly associated  
177 with age, cause of death, and technical batch, consistent with the findings of Parsana et al.  
178 (Parsana et al. 2019) (**Supplemental Fig. S5 I-L, Supplemental Fig. S6 C**). Thus regressing

179 PCs computed by accounting for tissue and cross-study heterogeneity from expression is integral  
180 to excluding technical effects and unwanted biological signals.

181 We examined the effect of PC-based data correction when inferring GCNs by aggregating  
182 data across diverse sources by comparing PC-based correction applied to either aggregate data,  
183 or individual studies followed by aggregation, where the number of PCs regressed is based on  
184 the permutation method described by Buja et. al (Buja and Eyuboglu 1992) and Leek et. al (Leek  
185 et al. 2012). Additionally, we compared the consequences of aggregating empirical covariance  
186 matrices inferred from PC-corrected data by either treating all studies irrespective of sample size  
187 equally (unweighted aggregation), or upweighting the covariance estimates from studies with a  
188 greater sample size (weighted aggregation). Thus, we used 4 paradigms: (1) Aggregating data  
189 before PC-based data correction followed by estimation of empirical covariance from residual  
190 expression, (2) PC-based data correction applied to individual studies followed by aggregation of  
191 residual expression and joint estimation of empirical covariance, (3) Unweighted aggregation of  
192 covariance matrices inferred from each study separately after study-specific PC-based correction  
193 and (4) Weighted aggregation of covariance matrices computed from individual studies  
194 following study-specific PC-based data correction, where the weights were the ratio of the study  
195 sample size to the total number of samples used in network reconstruction (**Fig. 2 A, Methods**).

196 To compare strategies, we split non-cancerous samples into two data splits, GTEx and  
197 SRA (**Supplemental Fig. S7**), followed by network inference by graphical lasso on one of the  
198 two data splits and evaluation with the held-out split by computing the held-out log-likelihood.  
199 Details pertaining to the number of studies, samples and median PCs regressed for incremental  
200 data aggregation are provided in **Supplemental Table S2**. Additionally, we assessed the  
201 recapitulation of known biological pathways by computing the F1-score of finding canonical

202 gene-gene relationships compiled from KEGG (Kanehisa and Goto 2000), Biocarta, and  
203 Pathway Interaction Database (Schaefer et al. 2009) obtained using Enrichr (Chen et al. 2013;  
204 Kuleshov et al. 2016) (**Supplemental Table S3**). Paradigms in which PC-based data correction  
205 preceded aggregation led to a strict increase in held-out log-likelihood and F1-scores of known  
206 gene relationships from canonical pathways with the addition of more studies (**Fig. 2 B, C,**  
207 **Supplemental Fig. S8, S9**). Additionally, we find that the low F1-scores were attributed to lower  
208 recall while the precision remained high, in accordance with previous studies that utilize  
209 graphical lasso to infer GCNs (Parsana et al. 2019). Further, we observed an increase in the  
210 precision with data aggregation for a particular value of recall across all strategies which  
211 performed PC-based data correction on individual studies (**Supplemental Fig. S10, S11**). This  
212 suggests that data aggregation resulted in GCNs with greater generalizability and recapitulated  
213 known biology better when technical confounders were estimated and regressed for individual  
214 studies. Since data aggregation led to a decrease in the number of edges found in the network for  
215 a particular value of the penalization parameter (**Supplemental Fig. S12**), we tested whether  
216 estimating denser networks would result in higher held-out log-likelihood specifically when the  
217 networks were inferred over a greater number of samples, but instead observed that a larger  
218 number of edges led to overfitting and lower generalizability (**Supplemental Fig. S13**). Further,  
219 the marginal improvement in network reconstruction diminished with the subsequent rounds of  
220 aggregation. While all methods that estimated technical confounders within each study  
221 performed similarly and were superior to estimating technical confounders across all samples  
222 when evaluated by held-out log-likelihood (**Fig. 2 D**), we found that weighted aggregation of  
223 covariance matrices led to a slight improvement in the F1-score of the networks when compared

224 to canonical pathways (**Fig. 2 E**), suggesting that this is the optimal strategy among the  
225 alternatives compared.

226 While our primary analysis concerns the recapitulation of individual, direct gene-gene  
227 edges through graphical lasso, which we expected to be heavily impacted by sample size, we  
228 also performed a limited evaluation of the effects of data aggregation with Weighted Gene  
229 Co-expression Network Analysis (WGCNA) (Langfelder and Horvath 2008), a popular method  
230 for identifying modules of co-expressed genes. We inferred WGCNA modules by sequentially  
231 aggregating GTEx tissues and SRA studies following PC correction (**Methods**). We discovered  
232 that data aggregation led to an improvement in the recapitulation of known gene relationships  
233 from KEGG (Kanehisa and Goto 2000), Biocarta, and Pathway Interaction Database (Schaefer et  
234 al. 2009) for both GTEx and SRA. However, we note that this improvement is not strictly  
235 monotonic, particularly at the highest levels of data aggregation, in contrast to graphical lasso.  
236 This may be expected as module detection for WGCNA combines information across multiple  
237 gene pairs to identify modules, and has been shown to work reasonably well even at small  
238 sample sizes. WGCNA module detection simply may not benefit as much from increased sample  
239 sizes. Thus, we conclude that PC-correction followed by data aggregation can potentially lead to  
240 an improvement in network performance for multiple network inference methods (**Supplemental**  
241 **Fig. S14**), but the improvement plateaus more quickly when inferring modules with WGCNA  
242 than when inferring direct edges with graphical lasso.

243 Finally, since graphical lasso can potentially identify edges reflecting direct gene-gene  
244 interactions, we evaluated the impact of data aggregation by weighted aggregation of covariance  
245 matrices which were estimated from SRA studies following PC correction on recapitulating  
246 known transcription factor (TF)-target gene relationships that were curated by Liska et. al (Liska

247 et al. 2022) based on experimental evidence such as ChIP-seq. We observed a modest  
248 improvement in the precision of predicting direct gene-gene relationships at higher values of  
249 recall with sequential data aggregation. While we do see improvement, the identification of direct  
250 gene interactions remains challenging in the presence of unknown technical and biological  
251 confounders (Kernfeld et al. 2024) (**Supplemental Fig. S15 A**).

252 We inferred consensus GCNs across diverse tissues by weighted aggregation of  
253 covariance matrices estimated from residual expression and graphical lasso (**Methods**). In  
254 addition to a universal consensus network which was inferred across 966 studies with sample  
255 size greater than or equal to 15, amounting to 95,276 samples across 48 tissue contexts, we  
256 constructed a non-cancer consensus network and a cancer consensus network. The non-cancer  
257 consensus network reflects data aggregated across 629 studies and 63,031 samples, and the  
258 cancer network reflects 386 studies and 29,967 samples (**Fig. 2 F**). The number of genes which  
259 were included in the inference of the three consensus networks is summarized in (**Supplemental**  
260 **Table S4**). We evaluated each consensus network to recapitulate previously reported gene-gene  
261 interaction using the F1 score. Across a range of network with a varying number of edges we  
262 obtained a higher estimate of the F1 score from the universal consensus network, followed by  
263 non-cancer and cancer consensus networks, which mirrors differences in sample size (**Fig. 2 G**).  
264 We observed that the universal consensus and non-cancer consensus networks performed better  
265 than the cancer consensus network at recapitulating potential TF-target relationships obtained  
266 from TFLink (version 1.0) (Liska et al. 2022), however, this could be either due to differences in  
267 sample size or the lack of cancer samples in the reference (**Supplemental Fig. S15 B**)

268 We inferred networks across 27 tissue contexts and examined the impact of data  
269 aggregation on context-specific network reconstruction by considering GTEx samples (GTEx

270 only) or by aggregating across samples from all data sources for that tissue context. The number  
271 of samples, studies, and median study-specific sample size for each tissue context in either  
272 aggregation setting are provided in **Supplemental Fig. S16**. The number of genes over which  
273 context-specific networks was inferred is summarized in (**Supplemental Table S4**). As in the  
274 consensus network inference, we used weighted aggregation of covariance matrices as the input  
275 to network inference by graphical lasso (**Methods**). To quantify the improvement in network  
276 reconstruction with data aggregation, we examined two tissue contexts with the largest sample  
277 size: blood and central nervous system (CNS). In both cases, we sequentially aggregated the  
278 blood or CNS SRA studies and computed the held-out log-likelihood utilizing context-matched  
279 GTEx samples. Similar to the results obtained from our consensus network analyses, we found  
280 that data aggregation led to a strict increase in held-out log-likelihood with additional studies and  
281 the greatest increase was observed while aggregating the first 20 studies (blood) and 15 studies  
282 (CNS) (**Methods, Fig. 2 H, I**). Further, we examined the impact of data aggregation on inferring  
283 a context-specific network, specifically, if PC-based data correction sufficiently accounts for  
284 inter-study heterogeneity and minimizes the discovery of false positives, while improving the  
285 detection of true positive edges, when compared to alternate approaches to minimize false  
286 positives such as tuning the penalization parameter to be sufficiently large. Thus we compared a  
287 blood-specific network inferred across all available samples to a blood-specific network inferred  
288 from a single study with a large sample-size (GTEx) in recapitulating known gene-gene  
289 interactions. We found that increasing the penalization parameter to improve the precision led to  
290 lower recall, a limitation that was overcome by data aggregation, which led to higher values of  
291 precision even for higher recall values. Finally, we observed that the optimal F1 score obtained

292 by data aggregation exceeded the optimal F1 score obtained by tuning the penalization parameter  
293 (**Supplemental Fig. S17**).

294       Orthogonally, we verified that our networks recapitulated known context-specific gene  
295 relationships by examining the enrichment of previously known tissue-specific protein-protein  
296 interactions (PPIs) from SNAP (Leskovec and Sosič 2016) in edges belonging to six tissue  
297 context-specific networks (adipose, blood, CNS, liver, lung, and skin) (**Methods**). Details of the  
298 SNAP PPI terms that were mapped to specific tissue-contexts can be found in **Supplemental**  
299 **Table S5**. Data aggregation and increased sample size in the network significantly increased the  
300 estimated odds ratio of tissue-specific PPIs in the liver (Median GTEx OR = 7.85, Median  
301 Aggregate OR = 38.85,  $p = 0.03$ ) and skin (Median GTEx OR = 21.83, Median Aggregated OR  
302 = 27.09,  $p = 0.05$ ), and there was weak enrichment in adipose (Median GTEx OR = 18.49,  
303 Median Aggregated OR = 21.14,  $p = 0.06$ ). In other tissue contexts, we observed a higher  
304 median odds ratio of PPI enrichment in networks inferred by data aggregation compared to  
305 GTEx-only networks (**Fig. 2 J**). Finally, we observed that context-specific networks obtained  
306 from blood, skin, central nervous system, liver, lung, and adipose were able to recapitulate  
307 known TF-target relationships from TFLink to varying degrees. The tissue with the highest  
308 number of samples, blood, resulted in networks with the best performance in reproducing  
309 TF-Target relationships as indicated by precision and recall (**Supplemental Fig. S15**). Thus, we  
310 demonstrated that data aggregation led to the improved inference of consensus networks that  
311 capture canonical gene interactions and tissue context-specific networks that capture tissue  
312 biology by observing better network generalizability and reproduction of known biological  
313 processes.

314 Central network nodes are evolutionarily constrained and include genes that are  
315 critical to tissue identity

316       The biological information captured by a GCN can be evaluated by comparing individual  
317 network edges, by examining whether there are edges between genes that are known to interact  
318 in a particular cellular pathway (Ha, Baladandayuthapani, and Do 2015), or by examining the  
319 properties of network nodes with a high number of connections or hubs (Pastor-Satorras, Rubi,  
320 and Diaz-Guilera 2003; Chou et al. 2014; Oh et al. 2015). Since eukaryotic transcriptional  
321 networks typically consist of a subset of genes, often transcription factors, that regulate many  
322 downstream target genes (Albert 2005), we chose specific values of the penalization parameter  $\lambda$   
323 and number of resulting network edges such that the selected networks are approximately  
324 scale-free (**Methods, Supplemental Fig. S18; Supplemental Table S6, Supplemental Table**  
325 **S7**). We computed different measures of centrality corresponding to each network node and  
326 tested for the enrichment of genes involved in GO terms that reflect ubiquitous or  
327 context-specific processes (**Supplemental Table S8**) among network nodes selected with  
328 progressively increasing thresholds for degree centrality against a background of all 18,882  
329 protein-coding genes (**Methods**). Central nodes from all three consensus networks were strongly  
330 enriched for genes involved in functions such as microtubule-based process, chromosome  
331 organization, and regulation of organelle organization (**Fig. 3 A, Supplemental Fig. S19**). In  
332 contrast, we found that central nodes from blood context-specific networks were enriched for  
333 genes associated with platelet activation, leukocyte differentiation, and leukocyte chemotaxis to a  
334 greater extent than central genes derived from either consensus or a discordant context-specific  
335 network (CNS) (**Fig. 3 B**). Further, these trends were reflected across multiple tissue contexts;  
336 context-specific networks corresponding to CNS (**Fig. 3 C**), skin, liver, and lung were enriched

337 for genes associated with tissue-matched GO terms (**Supplemental Fig. S20**). In addition, we  
338 examined the enrichment of central genes from tissue-specific gold standards obtained from  
339 HumanBase. We observed that network nodes with higher degree centrality were enriched for  
340 hub nodes (with a degree in the top 80<sup>th</sup> percentile) of concordant tissue-specific reference  
341 networks, as evidenced by an odds ratio  $> 1$  (**Supplemental Fig. S21**). Thus, while central genes  
342 from consensus networks included genes involved in essential cellular processes,  
343 context-specific gene relationships are lost with global aggregation and are unlikely to be  
344 recovered by increasing the sample size.

345       Next, we evaluated whether hub genes were evolutionarily constrained and whether they  
346 have known roles in complex traits or diseases (**Methods**). We first binned network nodes such  
347 that genes with a closeness centrality of 0 were assigned to Quintile 1, and those with at least 1  
348 connecting edge were grouped based on estimated quantiles of closeness centrality. We then  
349 computed the excess overlap of a particular gene set among network nodes binned by closeness  
350 centrality, as the ratio of the fraction of genes from the set found among the network nodes in a  
351 particular bin to the fraction of genes from the gene set found among all network nodes  
352 (**Methods**). Consensus network hub genes (Quintile 5) had a significantly higher excess overlap  
353 ( $>1$ ) with evolutionarily constrained gene sets than peripheral nodes (Quintiles 1-3), using  
354 metrics including high pLI genes, high  $s_{\text{het}}$  genes, and high missense Z-score genes. These trends  
355 were similar in context-specific networks with some variation in the strength of the trend across  
356 tissues likely driven by sample size differences and differential power in inferring these networks  
357 (**Fig. 3 D, Supplemental Fig. S22**). We then examined the enrichment of eQTL-deficient,  
358 ClinVar, OMIM, and FDA drug-targeted genes across quintiles of network centrality  
359 (**Supplemental Fig. S22, S23, Supplemental Table S9**). We observed that peripheral genes

360 (Quintile 1) and central genes (Quintile 5) of consensus networks exhibited an excess overlap  $> 1$   
361 of eQTL deficient genes (those which lacked significant *cis*-regulatory variants), while genes  
362 with intermediate connectivity were depleted of eQTL deficient genes, while the six  
363 context-specific networks had widely variable trends. While central genes from consensus  
364 networks were weakly depleted for OMIM and FDA drug-targeted genes, we observed an excess  
365 overlap  $> 1$  of hub genes belonging to context-specific networks. This could be explained by our  
366 earlier observations that central nodes from consensus networks were involved in essential and  
367 non-specific cellular processes while central nodes from context-specific networks were both  
368 specific and critical to tissue identity, thus, altering central consensus network hub nodes may  
369 have widespread and potentially deleterious off-target effects while context-specific hub nodes  
370 may identify targetable genes with tissue-specific effects. Finally, we observed that matched  
371 tissue-specific transcription factors (TFs) from Pierson et. al (Pierson et al. 2015) (**Supplemental**  
372 **Table S10**) had a significantly greater number of neighbors than 88 general TFs for  
373 context-specific networks corresponding to blood ( $p < 1e-4$ ), lung ( $p < 1e-4$ ), and skin ( $p < 0.01$ ),  
374 while in other tissues, except for CNS, the median degree of tissue-specific TFs was greater than  
375 general TFs and non-transcription factors (**Methods**). In contrast, while tissue-specific and  
376 general TFs had more neighbors in consensus networks when compared to non-transcription  
377 factors, we found no significant differences in the degree distribution of tissue-specific TFs to  
378 general TFs in either the universal or non-cancer consensus network (**Fig. 3 E**). Therefore, while  
379 both consensus and context-specific central genes were enriched for genes under high-selection  
380 pressure, context-specific hub nodes were more likely to be OMIM genes, drug targets and  
381 tissue-specific TFs.

382 We examined similarities and differences between network architectures of the  
383 non-cancer consensus and cancer consensus networks based on shared and distinct hub genes,  
384 since central genes are likely to be more relevant to network functionality (Pastor-Satorras, Rubi,  
385 and Diaz-Guilera 2003), and the identification of hubs has led to the discovery of genes involved  
386 in cancer (Chou et al. 2014; Oh et al. 2015), tissue regeneration (Rodius et al. 2016), and other  
387 diseases (Keller et al. 2008; Presson et al. 2008). Specifically, we found 296 shared hubs  
388 between cancer ( $\lambda = 0.24$ , 7552 edges) and non-cancer ( $\lambda = 0.18$ , 7,355 edges) consensus  
389 networks, and 312 hubs which were specific to the cancer consensus network (**Supplemental**  
390 **Table S11**). Cancer-specific hub genes were enriched for pathways such as ncRNA metabolic  
391 processing (GO:0034660,  $p = 5.2e-02$ ) which is believed to play a role in metabolic  
392 reprogramming in cancer, DNA damage response (GO:0006974,  $p = 1.17e-12$ ) which has been  
393 posited to play a role in cancer cell survival in non-optimal conditions, and response to ionizing  
394 radiation (GO:0010212,  $p = 6.1e-04$ ). Further, we found that cancer-specific hub genes were  
395 enriched for a plethora of DNA repair and replication pathways including, double-strand break  
396 repair via homologous recombination (GO:0000724,  $p = 6.36e-06$ ), recombinational repair  
397 (GO:0000725,  $p = 1.35e-06$ ), interstrand cross-link repair (GO:0036297,  $p = 5.48e-03$ ), and  
398 double-strand break repair via break-induced replication (GO:0000727,  $p = 1.36e-03$ )  
399 (**Supplemental File 1**).

400 To examine whether network properties were shared between related tissues we  
401 compared the overlap of hub, we considered all hub genes found in at least two tissue contexts  
402 ( $N=1,956$ ). Details of the penalization parameter selected for tissue-context specific networks  
403 used in this analysis are summarized in **Supplemental Table S12**. Grouping tissue contexts  
404 based on hub genes using non-negative matrix factorization with eight latent factors (**Methods**)

405 led to the grouping of related tissues such as blood and PBMCs/T cells (Factor 7) (**Fig. 3 F**,  
406 **Supplemental Table S13**). As expected, we found that hub genes that led to the grouping of  
407 blood and PBMCs/T cells were enriched for defense response (GO:0006952,  $p = 2.7 \times 10^{-24}$ ) and  
408 cytokine production (GO:0001816,  $p = 9.9 \times 10^{-7}$ ) (**Supplemental File 2**). Further, Factor 6 which  
409 led to the grouping of hESCs, iPSCs, and multipotent cells comprised of hub genes which were  
410 enriched for gastrulation (GO:0007369,  $p = 5.9 \times 10^{-4}$ ) and circulatory system development  
411 (GO:0072359,  $p = 6.2 \times 10^{-3}$ ) (**Supplemental File 3**).

412 Genes with high network centrality are proximal to variants enriched for complex  
413 trait heritability

414 Previous work by Kim et al. (Kim et al. 2019) reported that network topology annotations  
415 did not contribute to heritability once the LDSC baseline model (Finucane et al. 2015) was  
416 included. We examined whether data aggregation would increase the utility of network features  
417 for heritability analysis independently of baseline functional annotations. For each network we  
418 calculated centrality annotations by computing 6 different centrality measures including, degree,  
419 maximum weight, strength, closeness, betweenness, and PageRank. The correlation between the  
420 different centrality measures is summarized for select networks in **Supplemental Fig. S24**. We  
421 meta-analyzed estimates of heritability enrichment, the ratio of the proportion of heritability  
422 explained by SNPs belonging to an annotation to the proportion of SNPs in the annotation, and  
423  $\tau^*$ , an estimate of the heritability of SNPs unique to the annotation (Finucane et al. 2015), using a  
424 random effects model to obtain a summary of effect sizes estimated for a set of 42 independent  
425 traits considered by Kim et al. (**Methods, Supplemental Table S14**). We estimated both  
426 heritability enrichment and  $\tau^*$  by either conditioning an annotation corresponding to whether a

427 variant was located in a 100 kilobase window of all protein-coding genes (all-genes annotation),  
428 or conditioning on 97 functional annotations such as known enhancer and promoter regions  
429 which are included in the baseline-LD model and the all-genes annotation (all-genes + baseline).  
430 Similar to the results found by Kim et al., we observed a significant estimate  $\tau^*$  corresponding to  
431 our consensus network-derived annotations when conditioning on just the all-genes annotation,  
432 however, when conditioning on the baseline-LD model, the  $\tau^*$  observed for consensus  
433 network-derived annotations were no longer significant (**Fig. 4 A**). While we found no  
434 significant differences in enrichment across a varying number of edges present in the network  
435 when conditioned on the all-genes annotation, we observed that  $\tau^*$  decreased as the number of  
436 network edges decreased. There were no significant differences in either enrichment or  $\tau^*$  with  
437 the number of edges found in the network when conditioning on the baseline-LD annotations  
438 (**Supplemental Fig. S25**). Further, our observations were not dependent on the traits studied and  
439 remained consistent when we applied s-LDSC to 219 UKBB traits (**Supplemental Table S15**;  
440 **Supplemental Fig. S26**).

441 A possible explanation for the lack of heritability enrichment signal unique to network  
442 annotations is the redundancy between the baseline LD annotations and network topology  
443 annotations. Therefore, we hypothesized that context-specific data aggregation could prioritize  
444 variants enriched for heritability of concordant traits independent of baseline annotations. We  
445 applied s-LDSC to network centrality annotations derived from networks inferred only from  
446 GTEx blood samples (blood GTEx), networks inferred by aggregating recount3 blood samples  
447 (blood), and as a control, networks inferred by aggregating all samples (universal consensus), for  
448 a subset of 9 blood-related traits from the 42 independent traits (Crohn's disease, rheumatoid  
449 arthritis, ulcerative colitis, eosinophil count, platelet count, red blood cell count, red blood cell

450 width, white blood cell count, and eczema) (**Supplemental Table S16**). As with the consensus  
451 networks, tissue-specific networks displayed similar trends in heritability estimates with the  
452 number of edges found in the network (**Supplemental Fig. S27, S28**). When we conditioned on  
453 the baseline-LD annotations, we observed that annotations derived from the blood consensus  
454 networks had a significant  $\tau^*$  across all centrality annotations, while blood GTEx networks had a  
455 significant  $\tau^*$  for strength, degree, maximum weight and PageRank (**Fig. 4 B**). In contrast, we did  
456 not observe a significant  $\tau^*$  corresponding to annotations derived from the universal consensus  
457 network. We examined the generalizability of our results by conducting a similar experiment in  
458 CNS samples, another tissue with a large sample size. We applied s-LDSC to annotations derived  
459 from CNS networks inferred from GTEx samples (CNS GTEx), CNS networks inferred by  
460 aggregating samples from recount3 (CNS consensus), and the universal consensus networks for  
461 CNS-related traits which included waist-hip ratio adjusted BMI from the earlier set of 42 traits,  
462 as well as 7 traits from the Psychiatric Genomics Consortium (Alzheimer's, epilepsy, Parkinson's,  
463 bipolar disorder, smoking cessation, schizophrenia, major depressive disorder, and number of  
464 alcoholic drinks per week) (**Supplemental Table S17**). We found that annotations derived from  
465 both universal consensus and CNS-specific networks led to significant non-zero  $\tau^*$  when  
466 conditioning on the baseline-LD model. While we note that significant non-zero  $\tau^*$  was observed  
467 for the consensus networks for the chosen set of CNS traits in contrast to the 42 independent  
468 traits, possibly due to power, study quality, and other attributes of the GWAS, we found that  
469 annotations from tissue-specific networks led to significantly higher estimates of  $\tau^*$  and  
470 outperformed consensus networks (**Fig. 4 C**) for all centrality measures except closeness.  
471 Further, for betweenness, maximum weight, and PageRank centrality, CNS consensus networks

472 outperformed CNS GTEx networks, similar to the results in blood, demonstrating  
473 context-specific data aggregation results in network annotations that are enriched for trait  
474 heritability across tissue contexts. Across both sets of blood- and CNS-related traits, we found  
475 that PageRank centrality-derived annotations, which captured both the number of connections  
476 that a node has in addition to the centrality of its neighbors to determine the importance of a  
477 connection, performed consistently well. We conclude that context-specific aggregation results in  
478 the identification of the central genes of the network which are enriched for the heritability of  
479 concordant traits, and an increased sample size leads to a greater heritability enrichment signal.

## 480 **Discussion**

481 GCNs aid in determining changes in regulatory mechanisms that are key to cellular  
482 identity and prioritizing genes that drive phenotypic variability. However, conventional network  
483 analyses are often too underpowered to reliably discover gene-gene relationships and are  
484 compromised by spurious false positives and false negatives that result from limited power,  
485 noise, and unobserved technical confounders. We leveraged publicly available RNA-seq data  
486 from recount3 and manually curated tissue/cell type annotations to improve the inference of  
487 consensus and context-specific GCNs. Utilizing data splits, we demonstrated that accounting for  
488 confounders within individual studies followed by weighted aggregation of empirical covariance  
489 matrices led to the best improvement in network characteristics with data aggregation across  
490 multiple paradigms.

491 We then inferred three consensus networks (universal, non-cancer, and cancer networks)  
492 that recapitulated ubiquitous biological processes. Further, we aggregated data belonging to  
493 individual tissue contexts to infer 27 tissue context-specific networks that were enriched for

494 matched tissue-specific PPIs and shared similarities across related tissues. All networks and  
495 sample annotations are made publicly available as a resource for future studies.

496 Central genes from both consensus and context-specific networks were enriched for high  
497 PLI, and high Phi genes, indicating that hub genes are enriched for genes under high selective  
498 pressure. Context-specific hub genes were enriched for FDA-approved drug targets and OMIM  
499 genes while central genes from consensus networks which were inferred over a greater number  
500 of samples were depleted for both categories. Thus, context-specific information was lost by  
501 global aggregation, cannot be recovered by data aggregation or increased sample sizes, and is  
502 important to identifying drug targets and disease mechanisms. While the central genes of the  
503 network as determined by global data aggregation in the consensus network did not explain trait  
504 heritability independent of known functional annotations in the baseline-LD model, we found  
505 that context-specific data aggregation prioritized variants enriched for concordant trait  
506 heritability that did not overlap with previously known functional annotations. Thus topological  
507 properties of genes from context-specific GCNs hold significant promise as a functional  
508 annotation for identifying genetic variation that contributes to complex trait heritability.

509 A commonly used approach to identify genes associated with complex traits is to use  
510 colocalization analysis between GWAS and eQTL studies, however, often only about half of the  
511 signals colocalize with an eQTL (Mostafavi et al. 2023). Recent work by Mostafavi et al  
512 (Mostafavi et al. 2023) demonstrated that genes driving GWAS signals were often genes with  
513 complex context-dependent regulatory architecture and were depleted for eQTL variants. This  
514 has raised a call in the computational genomics community for orthogonal approaches to identify  
515 genes involved in complex traits. We found that annotations derived from context-specific GCNs  
516 are informative of trait heritability independent of context-agnostic functional annotations. This

517 suggests that tissue- and context-specific network centrality and other network properties could  
518 be used to help prioritize genes near GWAS loci (Zhu, Duren, and Wong 2021) or supplement  
519 eQTL data.

520         One of the major challenges in network inference remains the presence of unobserved  
521 technical confounders and undesirable biological signals which leads to spurious network edges  
522 and precludes causality claims. While PC-based data correction has been extensively utilized to  
523 reduce false positives resulting from confounding, recent work by Cote et. al (Cote, Young, and  
524 Huckins 2022) suggests that PC-based data correction, and related methods such as PEER  
525 (Stegle et al. 2012) and CONFETI (Ju et al. 2017), may over-correct expression data and remove  
526 biological co-expression of potential interest. Correcting or modeling confounders is essential to  
527 network accuracy, so tuning parameters such as the number of latent factors to correct as well as  
528 exploring alternative methods will continue to be important. Alternate approaches to handle  
529 confounding and infer causal regulatory relationships include instrumental variable analysis  
530 through the construction of local genetic instruments as outlined by Lujik et al. (Luijk et al.  
531 2018), however, since central network nodes are evolutionarily constrained and tightly regulated,  
532 it can be challenging to construct well-tracking genetic instruments for central genes,. Publicly  
533 available RNA-seq data including recount3, the extensive annotations we provide, and recent  
534 work which illustrated genotype calling using RNA-seq data (Deelen et al. 2015) could improve  
535 our ability to detect context-specific cis-regulatory effects, the reconstruction of local genetic  
536 instruments, and hence causal regulatory network inference.

537         Future directions aimed at improving GCN inference could leverage our extensively  
538 annotated sample characteristics and data aggregation strategies with complementary strategies  
539 including sharing information between related contexts (Omranian et al. 2016) to increase the

540 effective sample size, introducing constraints or priors corresponding to known regulatory  
541 relationships (Hellstern et al. 2021), and using alternate statistical measures of expression  
542 similarity that capture nonlinear associations between genes (Margolin et al. 2006). Additionally,  
543 heuristic algorithms such as the one proposed by Opgen-Rhein et al. (Opgen-Rhein and Strimmer  
544 2007) could be utilized to enrich our current networks with directionality information. Finally,  
545 while we studied tissue-contexts, we provide annotations of disease status which can be utilized  
546 to infer disease-specific GCNs.

547       Our finding that marginal improvement in network reconstruction decreases with  
548 continued data aggregation suggests that simply addressing statistical considerations due to  
549 sample size may have limitations for improving GCNs. Including orthogonal sources of  
550 information such as gene-enhancer associations inferred from Hi-C data (Babaei et al. 2015),  
551 transcription factor binding sites from ChIP-seq data (Zhou et al. 2016), and regulatory  
552 information derived from other epigenetic data types, in addition to gene expression quantified  
553 by RNA-seq in both bulk and single-cell studies, might result in a more accurate understanding  
554 of the shared regulatory architecture between genes. An example of integrating orthogonal  
555 information sources is found in recent work by Fu, X. et al. (Fu et al. 2025), which leverages  
556 paired scATAC-seq and snRNA-seq data across 213 fetal and adult cell types, along with prior  
557 knowledge of TF motifs to computationally infer local chromatin environments. The resulting  
558 model can then be used to predict gene expression in new cell types and TF regulators of  
559 downstream genes. This method and related approaches based on epigenetic data and TF motif  
560 information to infer targets of well-characterized TFs can be viewed as complementary to our  
561 approach, which is able to capture regulatory and co-expression relationships genome-wide  
562 based on large-scale RNA-seq data. Future methods may unify these approaches and incorporate

563 both sources of information. Additionally, experimental protocols such as Perturb-Seq (Dixit et  
564 al. 2016), which quantifies the transcriptional changes mediated by genetic manipulations on  
565 genes, processes, and states, could provide a new avenue for network inference and suggest  
566 causal mechanisms and edge directionality (Ota et al. 2025).

567 In conclusion, the growing availability of publicly shared RNA-seq data presents a  
568 valuable opportunity to improve gene GCN inference through data aggregation. While GCNs  
569 offer insights distinct from eQTL analyses and hold promise for uncovering the regulatory  
570 mechanisms underlying complex traits, their utility has been limited by challenges in data  
571 integration and variability across studies. In this work, we addressed these challenges by  
572 developing an approach that accounts for latent confounding and study-specific variability,  
573 enabling the construction of context-specific GCNs enriched for complex-trait heritability  
574 beyond baseline functional annotations.

## 575 **Methods**

### 576 Data pre-processing and quality control

577 We downloaded uniformly processed human RNA-seq samples using the recount3 R  
578 package (version 1.0.7; Wilks et al., 2021), running on R version 4.0.2 (R Core Team 2020)  
579 under Rocky Linux 8.8, and selected 1,747 projects that included 30 or more samples each (**Fig.**  
580 **1A**). Before normalization, we excluded samples with zero expression across all genes and genes  
581 that had zero expression across all samples in a project. We used in-built functions from the  
582 recount3 package to compute the RPKM transformed count matrix, selected genes that were  
583 protein-coding, autosomal, and unambiguously mapped to the reference genome (Battle 2019;  
584 Saha and Battle 2018), and generated the  $\log_2(RPKM + 1)$  count matrix for each project.

585           Following preliminary processing, we applied a unique data processing pipeline based on  
586 the data source. For projects belonging to GTEx, we excluded duplicates (labeled as  
587 STUDY\_NA), and samples derived from the chronic myelogenous leukemia (CML) cell line.  
588 We grouped samples by the tissue of origin to obtain 50 groups and 18,828 samples.

589           For TCGA, we excluded 67 samples missing sample type and 39 samples lacking patient  
590 ID. Replicates were identified as samples sharing both patient ID and sample type, and their gene  
591 expression was aggregated using the median. We grouped TCGA samples by cancer code,  
592 resulting in 33 groups and 11,091 samples.

593           For SRA, we first removed samples obtained via size fractionation. Replicates were  
594 defined by identical experiment accession numbers and aggregated using the median expression.  
595 Further, we excluded 89,101 samples where more than 50 percent of genes showed zero  
596 expression, which we used as a threshold to eliminate likely microRNA or degraded samples. To  
597 further restrict the dataset to bulk RNA-seq, we used predicted experiment-type labels from  
598 recount3 and excluded samples predicted as single-cell or small RNA-seq. If predicted labels  
599 were unavailable, we excluded samples with keywords such as “single cell,” “scRNA,”  
600 “snRNA,” or “single nucleus” in the study abstract. Additionally, we retained only those samples  
601 whose library selection metadata contained either cDNA or RT-PCR, when available. We also  
602 excluded studies which are known scRNA-seq experiments including: SRP096986, SRP135684,  
603 SRP166966, SRP200058, and SRP063998. For the remaining studies, we performed a text-based  
604 analysis to obtain the Study, Tissue, Organ, Biopsy, Cell, Disease, Source and Description from  
605 the metadata `sample_description` field. We then manually annotated 10,179 unique  
606 combinations of these fields to obtain tissue, cancer status, and disease type. In this manner, we

607 were able to obtain labels for 65,361 samples which we grouped on the basis of the study  
608 accession IDs to form 884 SRA studies (**Supplemental File 4**).

609 We grouped GTEx samples by tissue of origin, SRA samples by study accession ID, and  
610 TCGA samples by cancer accession code, and have referred to each individual group of samples  
611 as a “study” to simplify nomenclature. We did not distinguish on the basis of disease state or  
612 cancer status while organizing the data, until we proceeded to compute the inputs to network  
613 inference. The number of genes retained after filtering varied by study, particularly in smaller  
614 SRA projects with limited sample size. These gene count distributions are summarized in  
615 **Supplemental Fig. S1**.

#### 616 Identifying tissue type and cancer status

617

618 Wilks et. al (Wilks et al. 2021) demonstrated that for human bulk RNA-seq data, tissue or  
619 cell type of origin is the dominant source of gene expression variation, with clear tissue-specific  
620 clustering visible in the top four principal components. Building on this we manually refined  
621 annotated labels (**Supplemental File 4**) and grouped 95,484 samples and 5,999 genes (with  
622 non-zero variance) using t-SNE dimensionality reduction and clustering. Because cancerous and  
623 non-cancerous samples did not separate distinctly in the t-SNE space, we used manually  
624 annotated labels to restrict the analysis to 63,193 non-cancerous samples.

625 To maximize sample size, we merged similar tissues into broader tissue contexts  
626 (**Supplemental Table S1**), defined as a groups of samples with similar cell-type composition.  
627 Recognizing that gene expression can also vary due to technical factors such as batch effects and  
628 library size, we estimated the relative enrichment of 64 stromal and immune cell types using  
629 `xCell` gene signatures (Aran, Hu, and Butte 2017). Enrichment vectors for each sample were

630 then used for visualization and clustering via t-SNE, allowing us to group samples by shared  
631 cellular composition into distinct tissue contexts.

632 For 24 contexts with more than 500 samples, we removed outliers using six different  
633 outlier detection methods (**Supplemental Methods: Outlier calling methods to refine sample**  
634 **selection, Supplemental Fig. S2**). We examined whether selecting outliers based on any metric,  
635 including outliers labeled by 1, 2, or 3 metrics significantly impacted our estimate of the  
636 empirical covariance matrix from the data. We compared the frobenius norm of the differences in  
637 empirical covariance estimated for a particular tissue context with varying stringency on the  
638 inclusion criterion to the difference in the empirical covariance matrix estimated across contexts.  
639 We observed that the differences in the covariance estimates for varying the exclusion criterion  
640 were in general much smaller than the differences between two unrelated contexts, and hence we  
641 included samples within a tissue-specific context if it was labeled an outlier by 2 or fewer  
642 metrics to maximize the number of samples available for downstream analysis (**Supplemental**  
643 **Fig. S4**).

644 While this works with simpler tissue categories such as blood, skeletal muscle or colon  
645 where the samples have relatively homogenous cell type compositions, for the immune system,  
646 which comprises samples from the distinct myeloid, lymphoid and innate immune systems, these  
647 outlier metrics failed due to large intersample variation. Therefore for immune cell types, we first  
648 performed K-means clustering with 3 centroids using the in-built `kmeans()` function. We  
649 annotated the three resulting clusters based on the representation of manually annotated labels in  
650 each cluster as either B cells, myeloid cells (including monocytes and macrophages) and PBMCs  
651 w/ T cells (**Supplemental Fig. S3**). For each cluster, we performed outlier detection using all six  
652 methods outlined above and excluded samples that were found to be outliers in any two methods.

## 653 Data correction and aggregation

654 Principal component (PC) based correction methods can account for technical and  
655 biological artifacts that confound gene expression measurements and reduce false positives in  
656 gene network inference (Parsana et al. 2019). However, these methods have been applied to one  
657 experiment and not across multiple experiments from disparate sources. We systematically  
658 compared 4 strategies of data aggregation. In the first approach (aggregating data), expression  
659 data were pooled across all studies of interest, and confounders were estimated jointly from the  
660 combined dataset. This strategy reflects a global correction model in which confounding  
661 structure is assumed to be shared across datasets.

662 In the second approach (aggregating data adjusted for confounding), confounder  
663 correction was performed independently within each study before combining the corrected data.  
664 This addresses the possibility that latent structure differs across studies. The third and fourth  
665 approaches involved aggregating covariance matrices rather than gene expression matrices. In  
666 the unweighted aggregation of covariance matrices strategy, we treated each study equally and  
667 computed the average of study-level covariance matrices after within-study correction. In  
668 contrast, the weighted aggregation of covariance matrices strategy assumed that larger studies  
669 yield more reliable estimates, and we weighted each study's contribution by its sample size. Both  
670 approaches avoid direct normalization across heterogeneous datasets and instead pool structure  
671 at the level of gene–gene covariance. Complete implementation details for all four strategies are  
672 provided in the **Supplemental Methods: Detailed procedures for data correction and**  
673 **aggregation strategies.**

## 674 Network reconstruction with graphical lasso

675 Following the computation of aggregate covariance matrices using the strategies outlined  
 676 in **Supplemental Methods: Data correction and aggregation**, we inferred gene regulatory  
 677 relationships using graphical lasso (Friedman, Hastie, and Tibshirani 2008). The desired network  
 678 structure is obtained by identifying the precision matrix,  $\Theta = \Sigma^{-1}$  that maximizes the penalized  
 679 log-likelihood given by Eqn. 1, where  $C$  is the estimated covariance matrix.

$$680 \quad \hat{\Theta} = \underset{\Theta}{\operatorname{argmin}} \operatorname{tr}(C \cdot \Theta) - \log |\Theta| + \lambda \|\Theta\|_1 \quad \text{Eqn. 1}$$

681 We estimated the precision matrix  $\Theta$  across a range of  $\lambda$  between 0.04 to 1.00 in intervals of 0.02  
 682 using the R package QUIC (version 1.1.1). For genes  $p$  and  $q$ , an edge connecting them exists if  
 683 the corresponding entry in the precision matrix is non-zero as given by Eqn. 2

$$684 \quad \hat{N}_{p,q} = 1, \quad \text{if } |\hat{\Theta}_{p,q}| > 0$$

$$685 \quad 0, \quad \text{otherwise} \quad \text{Eqn. 2}$$

## 686 Network evaluation to determine the optimal aggregation strategy

687 To evaluate the impact of different data correction and aggregation strategies on network  
 688 quality, we applied all four approaches (see **Supplemental Methods: Detailed procedures for**  
 689 **data correction and aggregation strategies**) to non-cancerous samples from two partitions:  
 690 GTEx and SRA. GTEx samples were organized by tissue type, excluding tissues with fewer than  
 691 15 samples (e.g., Kidney Medulla), resulting in 49 tissue-level groups. For the SRA non-cancer  
 692 partition, we selected 566 studies with non-cancer annotations and at least 15 samples per study.

693 To assess how increasing sample size affects network performance, we constructed  
 694 aggregate networks by sequentially adding studies or tissues in order of increasing sample size.

695 For SRA, we evaluated networks at 1, 100, 200, 300, 400, 500, and all 566 studies. For GTEx,  
696 we tested 1, 10, 20, 30, 40, and 49 tissues. Each network was inferred using graphical lasso over  
697 a grid of penalization parameters between 0.04 and 1.00. **Supplemental Table S2** summarizes  
698 the number of samples, studies, median sample size, and principal components regressed at each  
699 aggregation level.

700 To compare network quality across aggregation strategies and sample sizes, we used two  
701 evaluation criteria: (1) held-out log-likelihood on independent datasets to measure  
702 generalizability and (2) biological validity based on (a) enrichment for known pathway  
703 co-membership and (b) transcription factor–target interactions. Precision, recall, and F1-score  
704 were computed for each network using standardized reference sets. Full computational details for  
705 all evaluation metrics are provided in the **Supplemental Methods: Detailed evaluation metrics**  
706 **to determine the impact of data aggregation**.

## 707 Network inference with WGCNA

708 To evaluate the effect of data aggregation on module-based gene co-expression networks,  
709 we used the WGCNA R package (Langfelder and Horvath 2008) version 1.72-5, (Langfelder and  
710 Horvath 2008). We constructed consensus networks by aggregating samples incrementally across  
711 three settings: (1) GTEx tissues in batches of 1, 3, 10, 30, and all 49 tissues; (2) non-cancerous  
712 SRA studies in batches of 1, 10, 20, 30, 100, 300, and all 566 studies; and (3) SRA studies  
713 annotated as blood in batches of 1, 20, 40, 60, and 65. For each aggregation level, we applied  
714 principal component correction to the individual studies or tissues before combining them. We  
715 retained only genes that were present in all datasets being aggregated. After performing standard  
716 WGCNA preprocessing, we estimated the adjacency matrix for each individual dataset using a  
717 power parameter selected to ensure approximate scale-free topology. Consensus networks were

718 then constructed by aggregating topological overlap matrices (TOMs) across studies. Modules  
719 were identified by hierarchical clustering followed by dynamic tree cutting from the WGCNA  
720 package, and similar modules were merged based on eigengene correlation. For each inferred  
721 network, we evaluated functional relevance by computing precision, recall, and F1-score based  
722 on known gene-gene interactions obtained by curating pathway information from KEGG,  
723 Biocarta and Pathway Interaction Database from Enrichr and selected those pathways that were  
724 annotated as canonical pathways by MSigDB.. Full computational procedures and parameter  
725 thresholds are provided in the **Supplemental Methods: Detailed procedure for**  
726 **WGCNA-based aggregation and evaluation.**

## 727 Inference of consensus and tissue context-specific networks

728 We inferred consensus networks across samples from disparate tissues and cell types to capture  
729 shared biological pathways across contexts. Since weighted covariance aggregation yielded the  
730 best performance among the four data correction and aggregation strategies, we grouped SRA  
731 samples by study accession ID, GTEx samples by tissue of origin, and TCGA samples by cancer  
732 code. We inferred the network structure over a range of penalization parameters from 0.08 to  
733 1.00. We constructed three types of consensus networks (universal, non-cancer, and cancer), each  
734 defined by different sample inclusion criteria (see **Supplemental Methods: Construction of**  
735 **consensus networks** for details).

736 We inferred context-specific networks in 27 contexts with 500 or more samples. Details  
737 of the number of samples, studies, and median sample size across studies for each context are  
738 provided in **Supplemental Fig. S16**. For 20 contexts including adipose, B cells, blood, breast,  
739 cardiac, central nervous system, colon, esophagus, fibroblasts, intestine, kidney, liver, lung,

740 nervous system, pancreas, prostate, skeletal muscle, skin, stomach, and vascular we inferred  
741 networks either using GTEx sample only or by aggregating context-specific samples from  
742 recount3 which included GTEx. For each context-specific network, we first performed PC-based  
743 data correction within each study followed by covariance estimation and aggregation by  
744 weighting the covariance matrix with the proportion of study-specific sample size to the total  
745 number of samples as detailed in **Supplemental Methods: Detailed procedures for data**  
746 **correction and aggregation strategies**. We then inferred GCNs using graphical lasso using Eqn.  
747 1 and Eqn. 2.

748 Evaluating the impact of data aggregation on the inference of consensus and  
749 context-specific networks

750 To evaluate whether aggregating samples across studies improves the performance of  
751 consensus and context specific networks, we computed the precision, recall, and F1 score of  
752 observing known gene co-regulatory relationships annotated in canonical biological pathways  
753 compiled across KEGG, Biocarta and the Pathway Interaction Database, as detailed in  
754 **Supplemental Methods: Detailed evaluation metrics to determine the impact of data**  
755 **aggregation**. For consensus networks we compared F1 scores across the universal, non-cancer,  
756 and cancer networks over a range of network sizes from 5,000 to 500,000 edges.

757 To test context-specific network performance we focused on the two largest contexts:  
758 blood and CNS. For each of these contexts, we sequentially aggregated SRA studies by  
759 increasing sample size and inferred networks. We then evaluated the generalizability of the  
760 networks inferred across varying numbers of samples by computing the held-out log-likelihood

761 using the corresponding GTEx tissues as held-out test sets (**Supplemental Methods:**  
762 **Computation of held-out log-likelihood for content-specific networks**).

763         Additionally, for 6 contexts (adipose, blood, CNS, liver, lung, and skin) we compared  
764 context specific networks constructed solely from GTEx to those derived through data  
765 aggregation by assessing the enrichment of tissue specific protein-protein interactions from the  
766 SNAP database. Odds ratios for enrichment were computed using Fisher's exact test. Additional  
767 statistical procedures, including two types of permutation testing and a Wilcoxon rank sum test  
768 for comparing aggregated versus GTEx only networks, are described in the **Supplemental**  
769 **Methods: Determining enrichment of known tissue-specific PPI interactions**.

#### 770 Sparsity parameter selection for consensus and context-specific networks

771 For each of the three consensus networks and 27 context specific networks, we evaluated the  
772 degree distribution of inferred networks across a range of penalization parameters. Specifically,  
773 we identified scale free networks as those where the degree distribution followed a power law  
774 with an estimated scaling exponent between 2 and 3 and a coefficient of determination ( $R^2$ )  
775 greater than 0.8. Additional methodological details, including model fitting and confidence  
776 interval calculations, are provided in the **Supplemental Methods: Detailed description of**  
777 **sparsity parameter selection**. Summary statistics and selected network parameters are reported  
778 in **Supplemental Tables S6 and S7**.

#### 779 Computing gene centrality measures based on network structure

780         We computed measures of network connectivity for each gene in the network with the  
781 `igraph` R package (version 1.3.5) (Csardi and Nepusz 2006). We used the absolute value of  
782 entries in the precision matrix (**Methods: Network reconstruction with graphical lasso**) to

783 define edge weights between genes and normalized these values by the maximum edge weight  
784 across the entire graph. Using these weights, we calculated gene-level centrality using several  
785 standard metrics: betweenness, closeness, degree, strength, maximum edge weight, and  
786 PageRank. For each gene, we used distance-based weights to compute betweenness and  
787 closeness centrality, while normalized edge weights were used for the remaining centrality  
788 measures. Details of how each centrality metric was computed, including mathematical formulas  
789 and algorithms used, are provided in the **Supplemental Methods: Computation of centrality**  
790 **measures**. Correlations between centrality measures across select networks are shown in  
791 **Supplemental Fig. S24**.

792 Enrichment of specific pathways among central genes in consensus and  
793 context-specific networks

794 To assess whether highly connected genes in inferred networks were enriched for known  
795 biological functions, we developed a general framework to test for the enrichment of functional  
796 gene sets among central genes. For each network, we estimated node degree (see **Methods:**  
797 **Computing gene centrality measures based on network structure**) and assessed functional  
798 enrichment at a series of increasing degree thresholds (**Supplemental Methods: Functional**  
799 **enrichment analysis of central genes**). For the consensus networks we first selected the value  
800 of the penalization parameter such that the resulting network had  $\sim 7,000$  edges. We then  
801 determined the odds ratio of finding genes belonging to ubiquitous biological processes among  
802 network nodes selected by successively increasing degree thresholds and compared the results to  
803 those obtained from blood and CNS-specific networks with a similar number of edges. Full

804 details of GO terms corresponding to ubiquitous biological processes is provided in  
805 **Supplemental Table S8**.

806 We extended this analysis to context-specific networks by selecting GO terms relevant to  
807 each context and testing for enrichment among high-degree nodes. For each of six contexts  
808 (blood, CNS, skin, lung, liver, and adipose), we selected one network inferred solely from GTEx  
809 samples and one inferred from aggregated samples (including GTEx) with ~7,000 edges. For  
810 example, in the blood context, we tested enrichment for GO terms such as leukocyte migration,  
811 leukocyte activation, and blood coagulation among high-degree nodes. As negative controls, we  
812 compared the observed enrichment in the blood-specific networks to that found in an unrelated  
813 context-specific network inferred across aggregated samples, as well as the universal and  
814 non-cancer consensus networks. A complete list of GO terms tested for each context is provided  
815 in **Supplemental Table S8**.

816 In a separate analysis, we compared inferred context specific networks to gold standard  
817 tissue specific networks from HumanBase (Greene et al. 2015). For each inferred network, we  
818 assigned nodes to degree-based bins and tested whether high-degree genes in our networks were  
819 enriched for hub genes (defined as those above the 80th percentile in degree) in the  
820 corresponding HumanBase network. Enrichment was tested across bins to assess the degree to  
821 which centrality in inferred networks aligns with regulatory importance in an external reference.  
822 Detailed procedures for these enrichment analyses are described in **Supplemental Methods:**  
823 **Enrichment of HumanBase hub nodes among central network nodes**.

824 Excess overlap of genes grouped by centrality measures with known evolutionarily  
825 constrained and functionally prioritized gene sets

826 We grouped genes for each consensus network such that the first bin includes genes with  
827 a closeness centrality of 0, the second bin contains nodes with closeness centrality in the lowest  
828 25<sup>th</sup> percentile, the third bin includes genes with closeness centrality in the 25<sup>th</sup> - 50<sup>th</sup> percentile,  
829 the fourth bin includes genes with closeness centrality in the 50<sup>th</sup> - 75<sup>th</sup> percentile and the fifth  
830 and final bin includes genes with closeness centrality greater than the 75<sup>th</sup> percentile.

831 For each bin, we computed the excess overlap with evolutionarily constrained and  
832 functionally prioritized gene sets as defined in Kim et al. (2019). We quantified enrichment by  
833 comparing genes in bin  $i$ ,  $G_b^i$  with each reference gene set  $j$ ,  $G_r^j$ , relative to the set of all genes  
834 in the network  $G_{tot}$ , using the following equations.

835 
$$P_d = \frac{|G_r^j \cap G_b^i|}{|G_b^i|} \quad \text{Eqn. 3}$$

836  
837 
$$P_{tot} = \frac{|G_r^j \cap G_{tot}|}{|G_{tot}|} \quad \text{Eqn. 4}$$

838  
839 
$$\text{excess overlap} (G_b^i, G_r^j) = \frac{P_d}{P_{tot}} \quad \text{Eqn. 5}$$

840  
841 
$$SE \text{ excess overlap} (G_b^i, G_r^j) = \sqrt{\frac{P_d(1-P_d)}{|G_b^i|}} / P_{tot} \quad \text{Eqn. 6}$$

842 Details on the reference gene sets are provided in the **Supplemental Methods:Reference gene**  
843 **sets used for overlap analysis** and in **Supplemental Table S9**.

844 Identifying biological processes associated with shared and distinct hub genes from  
845 non-cancer and cancer consensus network

846 In accordance with the scale-free criterion we selected the non-cancer network inferred  
847 using a penalization parameter  $\lambda = 0.18$  resulting in a network with 7,355 edges and the cancer  
848 consensus network corresponding to the penalization parameter  $\lambda = 0.24$  and a network with  
849 7,552 edges to compare the biological processes which are represented by shared and distinct  
850 network hubs. First, we defined hub genes as network nodes with a closeness centrality in the  
851 90th percentile independently for each consensus network, such that the non-cancer hub genes  
852 are given by  $H_N$  and the cancer hub genes are given by  $H_C$ . We then identified hub genes shared  
853 between cancer and non-cancer consensus networks  $H_S = H_N \cap H_C$ , non-cancer specific hub  
854 genes  $H_{NS} = H_N \cap H_C'$ , and cancer-specific hub genes as  $H_{CS} = H_C \cap H_N'$   
855 (**Supplemental Table S11**). We then used the `GOTermFinder` tool (Boyle et al. 2004) to  
856 identify GO terms that are shared by the genes in the sets  $H_S$ ,  $H_{NS}$ , and  $H_{CS}$ .

857 Examining the differences in the degree distribution of tissue-specific vs. general  
858 transcription factors in consensus and context-specific networks

859 We selected context-specific networks inferred from CNS, blood, cardiac, skin, lung,  
860 skeletal muscle, and pancreas samples from `recount3` which each had approximately 7,000 edges  
861 (**Supplemental Table S12**). Additionally, we selected values of the penalization parameter  $\lambda$   
862 which yielded universal and non-cancer consensus networks with  $\sim 7,000$  edges. We referred to  
863 Pierson et al. (Pierson et al. 2015) to obtain a list of tissue-specific and general transcription  
864 factors which are provided in **Supplemental Table S10**. To select a background set of non-TFs,

865 we first obtained the intersection of genes which were included in each network considered, then  
 866 we excluded both general and tissue-specific TFs from this list, and randomly selected 100 of  
 867 these genes. The selected background is provided in **Supplemental Table S10**. For each  
 868 network, we compared the degree distribution of tissue-specific and general transcription factors  
 869 to non-TFs and the degree distribution of tissue-specific to general transcription factors using the  
 870 Wilcoxon rank-sum test. Across all tests, we adjusted for multiple hypothesis correction using  
 871 the Holm-Bonferroni method.

872 Non-negative matrix factorization to determine shared co-regulatory relationships  
 873 in similar tissues

874 We selected context-specific networks with  $\sim 7,000$  edges across 27 contexts for which  
 875 we inferred GCNs by aggregating samples assigned to the context from recount3 (**Supplemental**  
 876 **Table S12**). Further, the selected networks were in accordance with the scale-free selection  
 877 criterion detailed in **Methods: Sparsity parameter selection for consensus and**  
 878 **context-specific networks**. For each network, we identified hub genes as network nodes with a  
 879 degree centrality in the 95th percentile. Across the 27 contexts, we found 3,682 unique hubs. We  
 880 subset to hubs that are present in at least 2 contexts which resulted in 1,956 hubs. We then used  
 881 the R package `RcppML` (version 0.3.7) to perform non-negative matrix factorization to learn 8  
 882 underlying factors to group similar patterns of hub genes. Specifically,  $H$  is a binary matrix of  
 883 dimensions  $N_{Hubs} \times N_c$ , where  $N_c$  is 27 the number of contexts.  $H_{i,j} = 1$  when the  $i^{th}$  gene is  
 884 a hub gene in context  $j$  and  $H_{i,j} = 0$  otherwise. We then obtain matrices  $W$  of dimensions  
 885  $N_{Hubs} \times 8$ , and  $C$  of dimensions  $N_c \times 8$  by solving the following optimization function,

886 
$$\min \|H - WC^T\| \text{ such that } W \geq 0, C \geq 0 \quad \text{Eqn. 25}$$

887 Finally, we chose a solution after 10 iterations that resulted in the greatest sparsity, i.e.  
 888 smallest values of  $\|W\|_1$  and  $\|C\|_1$ . To interpret the resulting context cluster, we examined the  
 889 genes that contributed the most to the corresponding factor. Specifically, for a given factor,  
 890  $W[:, p]$ , we first obtained genes with loadings in the 80% percentile. Then for each gene we  
 891 computed the maximum difference between the loading of the gene on factor  $p$  to all other  
 892 factors and selected genes where this difference is  $\geq 5 \times 10^{-5}$ . Thus we obtained a set of  
 893 factor-specific hub genes  $G_p$  (**Supplemental Table S13**). We then used the `GOTermFinder`  
 894 tool (Boyle et al. 2004) to identify GO terms that were more likely to be present in the set  $G_p$   
 895 than a background of all protein-coding genes by estimating the odds ratio and p-value by  
 896 applying the hypergeometric test.

897 Stratified LD-Score regression to quantify the heritability enrichment of variants  
 898 proximal to central network genes in consensus and context-specific networks

899 We applied stratified LD-score regression (s-LDSC) (Finucane et al. 2015) to assess  
 900 whether SNPs near central genes in inferred networks contributed disproportionately to complex  
 901 trait heritability. For the following networks, universal consensus, non-cancer consensus,  
 902 blood-specific (inferred from only GTEx data and across aggregated data from recount3), and  
 903 CNS-specific (inferred from only GTEx data and across aggregated data from recount3), we  
 904 obtained annotations corresponding to 6 different centrality measures, degree, betweenness,  
 905 closeness, strength, and PageRank (**Methods: Computing gene centrality measures based on**  
 906 **network structure**) by transforming the centrality scores to lie between 0 and 1. Each SNP was

907 annotated based on the centrality of genes within 100 kb, taking the maximum value when  
908 multiple genes were nearby. These annotations were tested for heritability enrichment and  
909 standardized effect ( $\tau_c^*$ ) using s-LDSC under two models, (1) one including only an all-genes  
910 annotation, and (2) another including the all-genes annotation and 97 annotations from the  
911 baseline-LD v2.2 model (Gazal et al. 2017; Hujoel et al. 2019; Villar et al. 2015; Marnetto et al.  
912 2018). Trait sets (**Supplemental Methods: Description of trait sets used in sLDSC**) included  
913 42 curated traits (Kim et al., 2019, **Supplemental Tables S14**), 219 UK Biobank traits  
914 (**Supplemental Tables S15**), 9 blood-related traits (**Supplemental Tables S16**), and 9  
915 CNS-related traits (**Supplemental Tables S17**). All networks used in the analysis satisfied the  
916 scale-free degree criterion (see **Methods: Sparsity parameter selection**). Final enrichment and  
917  $\tau_c^*$  estimates were summarized using random-effects meta-analysis by using the function  
918 `meta.summaries()` from the R package `rmeta` (version 3.0). Full procedural details and  
919 model specifications are provided in **Supplemental Methods: Stratified LD Score Regression**  
920 **Procedures**.

## 921 **Data access**

922 Scripts to reproduce the analysis and figures included in this manuscript are available in the  
923 Supplemental Code and can also be accessed at

924 [https://github.com/prashanthi-ravichandran/recount3\\_networks](https://github.com/prashanthi-ravichandran/recount3_networks)

925 Networks and annotations used in this project can be obtained from:

926 <https://zenodo.org/records/10480999>

## 927 **Competing interest statement**

928 A.B. is a consultant for Third Rock Ventures, LLC, a shareholder in Alphabet, Inc, and a founder of  
929 CellCipher, Inc.

## 930 **Acknowledgements**

931 The authors would like to thank helpful discussions from Battle lab members throughout the course of  
932 this work, particularly Joshua Weinstock and Eric Kernfeld for code review and manuscript feedback.

933 Alexis Battle was supported by NIH/NIGMS R35GM139580. Kaspar Hansen and Alexis Battle were  
934 supported by NIH/NIGMS R01GM121459.

### 935 **Authors' contributions**

936 P.R., P.P., and A.B. conceived the project. P.R., P.P., and A.B. designed the analyses. P.R. and P.P.

937 performed the analyses. R.K. and K.H. contributed feedback to experimental design and interpretation.

938 P.R., R.K., and A.B. organized and wrote the paper with input from all authors.

939 **References**

- 940 Albert, Réka. 2005. “Scale-Free Networks in Cell Biology.” *Journal of Cell Science*.  
 941 <https://doi.org/10.1242/jcs.02714>.
- 942 Alon, U. 2003. “Biological Networks: The Tinkerer as an Engineer.” *Science* 301 (5641): 1866–67.
- 943 Aran, Dvir, Zicheng Hu, and Atul J. Butte. 2017. “xCell: Digitally Portraying the Tissue Cellular  
 944 Heterogeneity Landscape.” *Genome Biology* 18 (1): 220.
- 945 Babaei, Sepideh, Ahmed Mahfouz, Marc Hulsman, Boudewijn P. F. Lelieveldt, Jeroen de Ridder, and  
 946 Marcel Reinders. 2015. “Hi-C Chromatin Interaction Networks Predict Co-Expression in the Mouse  
 947 Cortex.” *PLoS Computational Biology* 11 (5): e1004221.
- 948 Battle, Alexis. 2019. “Pre-Computed Cross-Mappability Resources for Human Genomes (hg19 and  
 949 GRCh38),” March. <https://doi.org/10.6084/m9.figshare.c.4297352.v4>.
- 950 Boyle, Elizabeth I., Shuai Weng, Jeremy Gollub, Heng Jin, David Botstein, J. Michael Cherry, and Gavin  
 951 Sherlock. 2004. “GO::TermFinder--Open Source Software for Accessing Gene Ontology  
 952 Information and Finding Significantly Enriched Gene Ontology Terms Associated with a List of  
 953 Genes.” *Bioinformatics* 20 (18): 3710–15.
- 954 Buja, A., and N. Eyuboglu. 1992. “Remarks on Parallel Analysis.” *Multivariate Behavioral Research* 27  
 955 (4): 509–40.
- 956 Chen, Edward Y., Christopher M. Tan, Yan Kou, Qiaonan Duan, Zichen Wang, Gabriela Vaz Meirelles,  
 957 Neil R. Clark, and Avi Ma’ayan. 2013. “Enrichr: Interactive and Collaborative HTML5 Gene List  
 958 Enrichment Analysis Tool.” *BMC Bioinformatics* 14 (April):128.
- 959 Chou, Wei-Chun, An-Lin Cheng, Marco Brotto, and Chun-Yu Chuang. 2014. “Visual Gene-Network  
 960 Analysis Reveals the Cancer Gene Co-Expression in Human Endometrial Cancer.” *BMC Genomics*  
 961 15 (April):300.
- 962 Cote, Alanna C., Hannah E. Young, and Laura M. Huckins. 2022. “Comparison of Confound Adjustment  
 963 Methods in the Construction of Gene Co-Expression Networks.” *Genome Biology* 23 (1): 44.
- 964 Csardi, Gabor, and Tamas Nepusz. 2006. “The Igraph Software Package for Complex Network  
 965 Research.” *InterJournal*. <https://igraph.org>.
- 966 Dam, Sipko van, Urmo Vösa, Adriaan van der Graaf, Lude Franke, and João Pedro de Magalhães. 2017.  
 967 “Gene Co-Expression Analysis for Functional Classification and Gene–disease Predictions.”  
 968 *Briefings in Bioinformatics* 19 (4): 575–92.
- 969 Deelen, Patrick, Daria V. Zhernakova, Mark de Haan, Marijke van der Sijde, Marc Jan Bonder, Juha  
 970 Karjalainen, K. Joeri van der Velde, et al. 2015. “Calling Genotypes from Public RNA-Sequencing  
 971 Data Enables Identification of Genetic Variants That Affect Gene-Expression Levels.” *Genome*  
 972 *Medicine* 7 (1): 30.
- 973 Diaz, Léo P. M., and Michael P. H. Stumpf. 2022. “Gaining Confidence in Inferred Networks.” *Scientific*  
 974 *Reports* 12. <https://doi.org/10.1038/s41598-022-05402-9>.
- 975 Dixit, Atray, Oren Parnas, Biyu Li, Jenny Chen, Charles P. Fulco, Livnat Jerby-Aron, Nemanja D.  
 976 Marjanovic, et al. 2016. “Perturb-Seq: Dissecting Molecular Circuits with Scalable Single-Cell RNA  
 977 Profiling of Pooled Genetic Screens.” *Cell* 167 (7): 1853–66.e17.
- 978 Finucane, Hilary K., Brendan Bulik-Sullivan, Alexander Gusev, Gosia Trynka, Yakir Reshef, Po-Ru Loh,  
 979 Verner Anttila, et al. 2015. “Partitioning Heritability by Functional Annotation Using Genome-Wide  
 980 Association Summary Statistics.” *Nature Genetics* 47 (11): 1228–35.
- 981 Friedman, Jerome, Trevor Hastie, and Robert Tibshirani. 2008. “Sparse Inverse Covariance Estimation  
 982 with the Graphical Lasso.” *Biostatistics* 9 (3): 432–41.
- 983 Fu, Xi, Shentong Mo, Alejandro Buendia, Anouchka P. Laurent, Anqi Shao, Maria del Mar  
 984 Alvarez-Torres, Tianji Yu, et al. 2025. “A Foundation Model of Transcription across Human Cell  
 985 Types.” *Nature* 637 (8047): 965–73.
- 986 Gazal, Steven, Hilary K. Finucane, Nicholas A. Furlotte, Po-Ru Loh, Pier Francesco Palamara, Xuanyao

- 987 Liu, Armin Schoech, et al. 2017. “Linkage Disequilibrium-Dependent Architecture of Human  
988 Complex Traits Shows Action of Negative Selection.” *Nature Genetics* 49 (10): 1421–27.
- 989 Greene, Casey S., Arjun Krishnan, Aaron K. Wong, Emanuela Ricciotti, Rene A. Zelaya, Daniel S.  
990 Himmelstein, Ran Zhang, et al. 2015. “Understanding Multicellular Function and Disease with  
991 Human Tissue-Specific Networks.” *Nature Genetics* 47 (6): 569–76.
- 992 Ha, Min Jin, Veerabhadran Baladandayuthapani, and Kim-Anh Do. 2015. “DINGO: Differential Network  
993 Analysis in Genomics.” *Bioinformatics* 31 (21): 3413–20.
- 994 Hartwell, L. H., J. J. Hopfield, S. Leibler, and A. W. Murray. 1999. “From Molecular to Modular Cell  
995 Biology.” *Nature* 402 (6761 Suppl): C47–52.
- 996 Hastie, Trevor, Robert Tibshirani, and Jerome Friedman. 2013. *The Elements of Statistical Learning:  
997 Data Mining, Inference, and Prediction*. Springer Science & Business Media.
- 998 Hasty, Jeff, David McMillen, and J. J. Collins. 2002. “Engineered Gene Circuits.” *Nature* 420 (6912):  
999 224–30.
- 1000 Hellstern, Michael, Jing Ma, Kun Yue, and Ali Shojaie. 2021. “Netgsa: Fast Computation and Interactive  
1001 Visualization for Topology-Based Pathway Enrichment Analysis.” *PLoS Computational Biology* 17  
1002 (6): e1008979.
- 1003 Huang, Yu-Jyun, Tzu-Pin Lu, and Chuhsing Kate Hsiao. 2020. “Application of Graphical Lasso in  
1004 Estimating Network Structure in Gene Set.” *Annals of Translational Medicine* 8 (23).  
1005 <https://doi.org/10.21037/atm-20-6490>.
- 1006 Hujoel, M. L. A., S. Gazal, F. Hormozdiari, B. van de Geijn, and A. L. Price. 2019. “Disease Heritability  
1007 Enrichment of Regulatory Elements Is Concentrated in Elements with Ancient Sequence Age and  
1008 Conserved Function across Species.” *American Journal of Human Genetics* 104 (4).  
1009 <https://doi.org/10.1016/j.ajhg.2019.02.008>.
- 1010 Ju, Jin Hyun, Sushila A. Shenoy, Ronald G. Crystal, and Jason G. Mezey. 2017. “An Independent  
1011 Component Analysis Confounding Factor Correction Framework for Identifying Broad Impact  
1012 Expression Quantitative Trait Loci.” *PLoS Computational Biology* 13 (5): e1005537.
- 1013 Kanehisa, M., and S. Goto. 2000. “KEGG: Kyoto Encyclopedia of Genes and Genomes.” *Nucleic Acids  
1014 Research* 28 (1): 27–30.
- 1015 Katz, Kenneth, Oleg Shutov, Richard Lapoint, Michael Kimelman, J. Rodney Brister, and Christopher  
1016 O’Sullivan. 2022. “The Sequence Read Archive: A Decade More of Explosive Growth.” *Nucleic  
1017 Acids Research* 50 (D1): D387–90.
- 1018 Keller, Mark P., Younjeong Choi, Ping Wang, Dawn Belt Davis, Mary E. Rabaglia, Angie T. Oler, Donald  
1019 S. Stapleton, et al. 2008. “A Gene Expression Network Model of Type 2 Diabetes Links Cell Cycle  
1020 Regulation in Islets with Diabetes Susceptibility.” *Genome Research* 18 (5): 706–16.
- 1021 Kernfeld, Eric, Rebecca Kenner, Alexis Battle, and Patrick Cahan. 2024. “Transcriptome Data Are  
1022 Insufficient to Control False Discoveries in Regulatory Network Inference.” *Cell Systems* 15 (8):  
1023 709–24.e13.
- 1024 Kim, Samuel S., Chengzhen Dai, Farhad Hormozdiari, Bryce van de Geijn, Steven Gazal, Yongjin Park,  
1025 Luke O’Connor, et al. 2019. “Genes with High Network Connectivity Are Enriched for Disease  
1026 Heritability.” *American Journal of Human Genetics* 105 (6): 1302.
- 1027 Kodama, Y., M. Shumway, R. Leinonen, and on behalf of the International Nucleotide Sequence Database  
1028 Collaboration. 2012. “The Sequence Read Archive: Explosive Growth of Sequencing Data.” *Nucleic  
1029 Acids Research*. <https://doi.org/10.1093/nar/gkr854>.
- 1030 Kuleshov, Maxim V., Matthew R. Jones, Andrew D. Rouillard, Nicolas F. Fernandez, Qiaonan Duan,  
1031 Zichen Wang, Simon Koplev, et al. 2016. “Enrichr: A Comprehensive Gene Set Enrichment Analysis  
1032 Web Server 2016 Update.” *Nucleic Acids Research* 44 (W1): W90–97.
- 1033 Langfelder, Peter, and Steve Horvath. 2008. “WGCNA: An R Package for Weighted Correlation Network  
1034 Analysis.” *BMC Bioinformatics* 9 (1): 1–13.
- 1035 Leek, Jeffrey T., W. Evan Johnson, Hilary S. Parker, Andrew E. Jaffe, and John D. Storey. 2012. “The Sva  
1036 Package for Removing Batch Effects and Other Unwanted Variation in High-Throughput  
1037 Experiments.” *Bioinformatics*. <https://doi.org/10.1093/bioinformatics/bts034>.

- 1038 Leskovec, Jure, and Rok Sosič. 2016. “SNAP: A General Purpose Network Analysis and Graph Mining  
1039 Library.” *ACM Transactions on Intelligent Systems and Technology* 8 (1).  
1040 <https://doi.org/10.1145/2898361>.
- 1041 Liska, Orsolya, Balázs Bohár, András Hidas, Tamás Korcsmáros, Balázs Papp, Dávid Fazekas, and Eszter  
1042 Ari. 2022. “TFLink: An Integrated Gateway to Access Transcription Factor–target Gene Interactions  
1043 for Multiple Species.” *Database: The Journal of Biological Databases and Curation* 2022  
1044 (September):baac083.
- 1045 Luijk, René, Koen F. Dekkers, Maarten van Iterson, Wibowo Arindrarto, Annique Claringbould, Paul  
1046 Hop, Dorret I. Boomsma, et al. 2018. “Genome-Wide Identification of Directed Gene Networks  
1047 Using Large-Scale Population Genomics Data.” *Nature Communications* 9 (1): 3097.
- 1048 Margolin, Adam A., Ilya Nemenman, Katia Basso, Chris Wiggins, Gustavo Stolovitzky, Riccardo Dalla  
1049 Favera, and Andrea Califano. 2006. “ARACNE: An Algorithm for the Reconstruction of Gene  
1050 Regulatory Networks in a Mammalian Cellular Context.” *BMC Bioinformatics* 7 (1): 1–15.
- 1051 Marnetto, Davide, Federica Mantica, Ivan Molineris, Elena Grassi, Igor Pesando, and Paolo Provero.  
1052 2018. “Evolutionary Rewiring of Human Regulatory Networks by Waves of Genome Expansion.”  
1053 *American Journal of Human Genetics* 102 (2): 207–18.
- 1054 Mostafavi, Hakhamanesh, Jeffrey P. Spence, Sahin Naqvi, and Jonathan K. Pritchard. 2023. “Systematic  
1055 Differences in Discovery of Genetic Effects on Gene Expression and Complex Traits.” *Nature*  
1056 *Genetics* 55 (11): 1866–75.
- 1057 Narang, Vipin, Muhamad Azfar Ramli, Amit Singhal, Pavanish Kumar, Gennaro de Libero, Michael  
1058 Poidinger, and Christopher Monterola. 2015. “Automated Identification of Core Regulatory Genes in  
1059 Human Gene Regulatory Networks.” *PLoS Computational Biology* 11 (9): e1004504.
- 1060 Oh, Eun-Yeong, Stephen M. Christensen, Sindhu Ghanta, Jong Cheol Jeong, Octavian Bucur, Benjamin  
1061 Glass, Laleh Montaser-Kouhsari, et al. 2015. “Extensive Rewiring of Epithelial-Stromal  
1062 Co-Expression Networks in Breast Cancer.” *Genome Biology* 16 (1): 128.
- 1063 Oltvai, Zoltán N., and Albert-László Barabási. 2002. “Systems Biology. Life’s Complexity Pyramid.”  
1064 *Science* 298 (5594): 763–64.
- 1065 Omranian, Nooshin, Jeanne M. O. Eloundou-Mbebi, Bernd Mueller-Roeber, and Zoran Nikoloski. 2016.  
1066 “Gene Regulatory Network Inference Using Fused LASSO on Multiple Data Sets.” *Scientific*  
1067 *Reports* 6 (February):20533.
- 1068 Opgen-Rhein, Rainer, and Korbinian Strimmer. 2007. “From Correlation to Causation Networks: A  
1069 Simple Approximate Learning Algorithm and Its Application to High-Dimensional Plant Gene  
1070 Expression Data.” *BMC Systems Biology* 1 (August):37.
- 1071 Ota, Mineto, Jeffrey P. Spence, Tony Zeng, Emma Dann, Alexander Marson, and Jonathan K. Pritchard.  
1072 2025. “Causal Modeling of Gene Effects from Regulators to Programs to Traits: Integration of  
1073 Genetic Associations and Perturb-Seq.” *bioRxiv*. <https://doi.org/10.1101/2025.01.22.634424>.
- 1074 Parsana, Princy, Claire Ruberman, Andrew E. Jaffe, Michael C. Schatz, Alexis Battle, and Jeffrey T.  
1075 Leek. 2019. “Addressing Confounding Artifacts in Reconstruction of Gene Co-Expression  
1076 Networks.” *Genome Biology* 20 (1): 94.
- 1077 Pastor-Satorras, Romualdo, Miguel Rubi, and Albert Diaz-Guilera. 2003. *Statistical Mechanics of*  
1078 *Complex Networks*. Springer Science & Business Media.
- 1079 Pierson, Emma, GTEx Consortium, Daphne Koller, Alexis Battle, Sara Mostafavi, Kristin G. Ardlie, Gad  
1080 Getz, et al. 2015. “Sharing and Specificity of Co-Expression Networks across 35 Human Tissues.”  
1081 *PLoS Computational Biology* 11 (5): e1004220.
- 1082 Presson, Angela P., Eric M. Sobel, Jeanette C. Papp, Charlyn J. Suarez, Toni Whistler, Mangalathu S.  
1083 Rajeevan, Suzanne D. Vernon, and Steve Horvath. 2008. “Integrated Weighted Gene Co-Expression  
1084 Network Analysis with an Application to Chronic Fatigue Syndrome.” *BMC Systems Biology* 2  
1085 (November):95.
- 1086 R Core Team. 2020. *R: A Language and Environment for Statistical Computing* (version 4.0.2).
- 1087 Rodius, Sophie, Anna Fournier, Lou Götz, Robin Liechti, Isaac Crespo, Susanne Merz, Petr V. Nazarov,  
1088 et al. 2016. “Analysis of the Dynamic Co-Expression Network of Heart Regeneration in the

- 1089 Zebrafish.” *Scientific Reports* 6 (May):26822.
- 1090 Saha, Ashis, and Alexis Battle. 2018. “False Positives in Trans-eQTL and Co-Expression Analyses  
1091 Arising from RNA-Sequencing Alignment Errors.” *F1000Research* 7 (November):1860.
- 1092 Schaefer, Carl F., Kira Anthony, Shiva Krupa, Jeffrey Buchoff, Matthew Day, Timo Hannay, and Kenneth  
1093 H. Buetow. 2009. “PID: The Pathway Interaction Database.” *Nucleic Acids Research* 37 (Database  
1094 issue): D674–79.
- 1095 Schlitt, Thomas, Kimmo Palin, Johan Rung, Sabine Dietmann, Michael Lappe, Esko Ukkonen, and Alvis  
1096 Brazma. 2003. “From Gene Networks to Gene Function.” *Genome Research* 13 (12): 2568–76.
- 1097 Segal, E., M. Shapira, A. Regev, D. Pe’er, D. Botstein, D. Koller, and N. Friedman. 2003. “Module  
1098 Networks: Identifying Regulatory Modules and Their Condition-Specific Regulators from Gene  
1099 Expression Data.” *Nature Genetics* 34 (2). <https://doi.org/10.1038/ng1165>.
- 1100 Stegle, Oliver, Leopold Parts, Matias Piipari, John Winn, and Richard Durbin. 2012. “Using Probabilistic  
1101 Estimation of Expression Residuals (PEER) to Obtain Increased Power and Interpretability of Gene  
1102 Expression Analyses.” *Nature Protocols* 7 (3): 500–507.
- 1103 Stuart, Joshua M., Eran Segal, Daphne Koller, and Stuart K. Kim. 2003. “A Gene-Coexpression Network  
1104 for Global Discovery of Conserved Genetic Modules.” *Science*, October.  
1105 <https://doi.org/10.1126/science.1087447>.
- 1106 The GTEx Consortium. 2020. “The GTEx Consortium Atlas of Genetic Regulatory Effects across Human  
1107 Tissues.” *Science*. <https://doi.org/10.1126/science.aaz1776>.
- 1108 Tomczak, Katarzyna, Patrycja Czerwińska, and Maciej Wiznerowicz. 2015. “The Cancer Genome Atlas  
1109 (TCGA): An Immeasurable Source of Knowledge.” *Contemporary Oncology* 19 (1A): A68–77.
- 1110 Villar, Diego, Camille Berthelot, Sarah Aldridge, Tim F. Rayner, Margus Lukk, Miguel Pignatelli,  
1111 Thomas J. Park, et al. 2015. “Enhancer Evolution across 20 Mammalian Species.” *Cell* 160 (3):  
1112 554–66.
- 1113 Wang, Xuran, David Choi, and Kathryn Roeder. 2021. “Constructing Local Cell-Specific Networks from  
1114 Single-Cell Data.” *Proceedings of the National Academy of Sciences of the United States of America*  
1115 118 (51). <https://doi.org/10.1073/pnas.2113178118>.
- 1116 Wilks, Christopher, Shijie C. Zheng, Feng Yong Chen, Rone Charles, Brad Solomon, Jonathan P. Ling,  
1117 Eddie Luidy Imada, et al. 2021. “recount3: Summaries and Queries for Large-Scale RNA-Seq  
1118 Expression and Splicing.” *Genome Biology* 22 (1): 323.
- 1119 Wolf, Denise M., Marc E. Lenburg, Christina Yau, Aaron Boudreau, and Laura J. van ‘t Veer. 2014.  
1120 “Gene Co-Expression Modules as Clinically Relevant Hallmarks of Breast Cancer Diversity.” *PloS*  
1121 *One* 9 (2). <https://doi.org/10.1371/journal.pone.0088309>.
- 1122 Zhou, Ke-Ren, Shun Liu, Wen-Ju Sun, Ling-Ling Zheng, Hui Zhou, Jian-Hua Yang, and Liang-Hu Qu.  
1123 2016. “ChIPBase v2.0: Decoding Transcriptional Regulatory Networks of Non-Coding RNAs and  
1124 Protein-Coding Genes from ChIP-Seq Data.” *Nucleic Acids Research* 45 (D1): D43–50.
- 1125 Zhu, Xiang, Zhana Duren, and Wing Hung Wong. 2021. “Modeling Regulatory Network Topology  
1126 Improves Genome-Wide Analyses of Complex Human Traits.” *Nature Communications* 12 (1):  
1127 1–15.

## 1128 Figure Legends

1129 **Figure 1: Overview of data pre-processing and annotations (A)** Gene expression data was  
1130 RPKM normalized and log-transformed along with gene-specific and sample-specific filters.  
1131 Based on the data source, normalized gene expression was processed to merge replicates and  
1132 exclude miRNA and scRNA seq samples. **(B)** Number of samples which were annotated to be  
1133 non-cancer and cancer based on available metadata across GTEx, SRA, and TCGA. 63 SRA  
1134 samples did not have an associated annotation corresponding to cancer status. **(C)** Top 10 tissue  
1135 labels by sample size across all three data sources: SRA, GTEx, and TCGA. **(D)** Top 20 diseases

1136 by sample size found in SRA that are not cancer. **(E)** t-SNE projection of xCell deconvolution  
 1137 scores of 63,193 non-cancerous samples colored by the tissue of origin. **(F)** Increase in the  
 1138 sample size of 27 tissue contexts by using SRA samples compared to GTEx only. SRA studies  
 1139 included 7 novel contexts which were not available in GTEx.

1140

1141 **Figure 2: Comparison of aggregation strategies to optimize network reconstruction (A)**

1142 Outline of strategies to compare data correction before and after aggregation and weighted and  
 1143 unweighted aggregation of single tissue/ study covariance matrices included (1) Aggregating  
 1144 data before PC-based data correction followed by estimation of empirical covariance from  
 1145 residual expression (Aggregating data, orange), (2) PC-based data correction applied to  
 1146 individual studies followed by aggregation of residual expression and joint estimation of  
 1147 empirical covariance (Aggregating data adjusted for confounding, brick red), (3) Unweighted  
 1148 aggregation of covariance matrices inferred from each study separately after study-specific  
 1149 PC-based correction (Unweighted covariance aggregation, purple) and (4) Weighted aggregation  
 1150 of covariance matrices computed from individual studies following study-specific PC-based data  
 1151 correction (Weighted covariance aggregation, magenta). **(B)** Held-out log-likelihood of networks  
 1152 inferred by sequentially aggregating either 10 GTEx studies or 100 SRA studies at a time vs. the  
 1153 log of the number of edges ( $|E|$ ) found in networks obtained by varying the penalization  
 1154 parameter  $\lambda$  **(C)** F1-score of networks inferred by sequentially aggregating either 10 GTEx  
 1155 studies or 100 SRA studies at a time vs. the log of the number of edges ( $|E|$ ) found in networks  
 1156 obtained by varying the penalization parameter  $\lambda$  when compared to canonical pathways  
 1157 compiled from KEGG, Biocarta, and Pathway Interaction Database. **(D)** Comparison of held-out  
 1158 log-likelihood corresponding to networks inferred over 49 GTEx studies or 566 SRA studies vs.  
 1159 the log of the number of edges ( $|E|$ ) found in networks obtained by varying the penalization  
 1160 parameter  $\lambda$  using four different aggregation strategies including aggregating data, aggregating  
 1161 data adjusted for confounding, unweighted, and weighted aggregation of covariance matrices.  
 1162 **(E)** Comparison of F1-scores of obtaining edges corresponding to canonical pathways from  
 1163 KEGG, Biocarta, and Pathway Interaction Database in networks inferred over 49 GTEx studies  
 1164 or 566 SRA studies vs. the log of the number of edges ( $|E|$ ) found in networks obtained by  
 1165 varying the penalization parameter  $\lambda$  using four different aggregation strategies including  
 1166 aggregating data, aggregating data adjusted for confounding, unweighted, and weighted  
 1167 aggregation of covariance matrices. **(F)** Total number of samples, number of individual studies,  
 1168 and the median sample size of each study which were used in the inference of universal  
 1169 consensus, non-cancer consensus, and cancer consensus networks. **(G)** Comparison of F1-scores  
 1170 of obtaining edges corresponding to canonical pathways in the three consensus networks,  
 1171 universal, non-cancer, and cancer, across networks with number of edges ( $|E|$ ) varying between  
 1172  $5 \times 10^3$  to  $5 \times 10^6$  edges. **(H)** Log-likelihood of GTEx blood samples based on networks  
 1173 inferred by sequentially aggregating SRA blood studies five at a time for number of edges  
 1174 ranging from  $10^3$  to  $10^5$  edges. **(I)** Log-likelihood of GTEx CNS samples based on networks  
 1175 inferred by sequentially aggregating SRA CNS studies five at a time for number of edges  
 1176 ranging from  $10^3$  to  $10^5$  edges. **(J)** Odds ratio of finding edges corresponding to tissue-specific  
 1177 protein-protein interactions (PPIs) derived from SNAP in tissue-context-specific networks  
 1178 inferred using all available samples vs. only samples found in GTEx for six tissue contexts.

1179

1180 **Figure 3: Properties of central network nodes of consensus and context-specific networks**

1181 **(A-C)** Enrichment of genes involved in GO processes among network genes selected with

1182 increasing thresholds of node degree in three consensus networks, universal ( $\lambda = 0.18$ , 7087  
 1183 edges), non-cancer ( $\lambda = 0.18$ , 7355 edges), and cancer ( $\lambda = 0.24$ , 7552 edges), as well as two  
 1184 context-specific networks blood ( $\lambda = 0.24$ , 7283 edges) and CNS ( $\lambda = 0.28$ , 8430 edges).  
 1185 Tissue-context-specific networks were inferred only using non-cancerous samples. Blood  
 1186 (GTEx) or CNS (GTEx) networks were inferred using samples only found in GTEx while Blood  
 1187 and CNS networks were inferred using samples from GTEx and SRA. **(D)** Distribution of the  
 1188 excess overlap of evolutionarily conserved gene sets (Methods) for network nodes binned by the  
 1189 number of neighbors (degree) corresponding to universal consensus networks ( $\lambda = 0.14$ , 0.16,  
 1190 0.18, 0.20), non-cancer consensus network ( $\lambda = 0.14$ , 0.16, 0.18, 0.20), cancer consensus  
 1191 networks ( $\lambda = 0.20$ , 0.22, 0.24, 0.26), blood network ( $\lambda = 0.18$ , 0.20, 0.22, 0.24, 0.26), and CNS  
 1192 network ( $\lambda = 0.24$ , 0.26, 0.28, 0.30, 0.32). Quintile 1 reflects nodes with no neighbors. Nodes  
 1193 with non-zero neighbors are split based on the degree quartile they belong to (Quintiles 2-5). We  
 1194 evaluated the excess overlap of 3,104 loss-of-function (LoF) genes with pLI > 0.9, 2,853 genes  
 1195 with a  $S_{\text{het}} > 0.1$ , 588 genes with a Phi-score > 0.95, and 1,440 genes strongly depleted for  
 1196 missense mutations (high missense z-score). **(E)** The degree distribution of network nodes that  
 1197 are tissue-specific transcription factors (TFs) in blood (52 TFs), lung (58 TFs), skin (10 TFs),  
 1198 pancreas (16 TFs), cardiac (17 TFs), muscle (7 TFs), CNS (51 TFs), general transcription factors  
 1199 (88 TFs), and protein-coding genes which are not transcription factors in universal consensus ( $\lambda$   
 1200 = 0.18, 7,087 edges), non-cancer consensus ( $\lambda = 0.18$ , 7,355 edges), skin ( $\lambda = 0.26$ , 7,567 edges),  
 1201 skeletal muscle ( $\lambda = 0.26$ , 6,254 edges), pancreas ( $\lambda = 0.32$ , 7,615 edges), lung ( $\lambda = 0.30$ , 6,349  
 1202 edges), CNS ( $\lambda = 0.30$ , 6,316 edges), cardiac ( $\lambda = 0.30$ , 6,481 edges), blood ( $\lambda = 0.24$ , 7,283  
 1203 edges). Pairs with no significance reported were not statistically distinct ( $p > 0.1$ ). **(F)** Factor  
 1204 weights were obtained by non-negative matrix factorization of the presence of hub genes in  
 1205 tissue-specific networks with ~ 7,000 edges. Details of the penalization parameter  $\lambda$  and the  
 1206 number of edges of selected networks for each tissue context are provided in **Supplemental**  
 1207 **Table S7**.

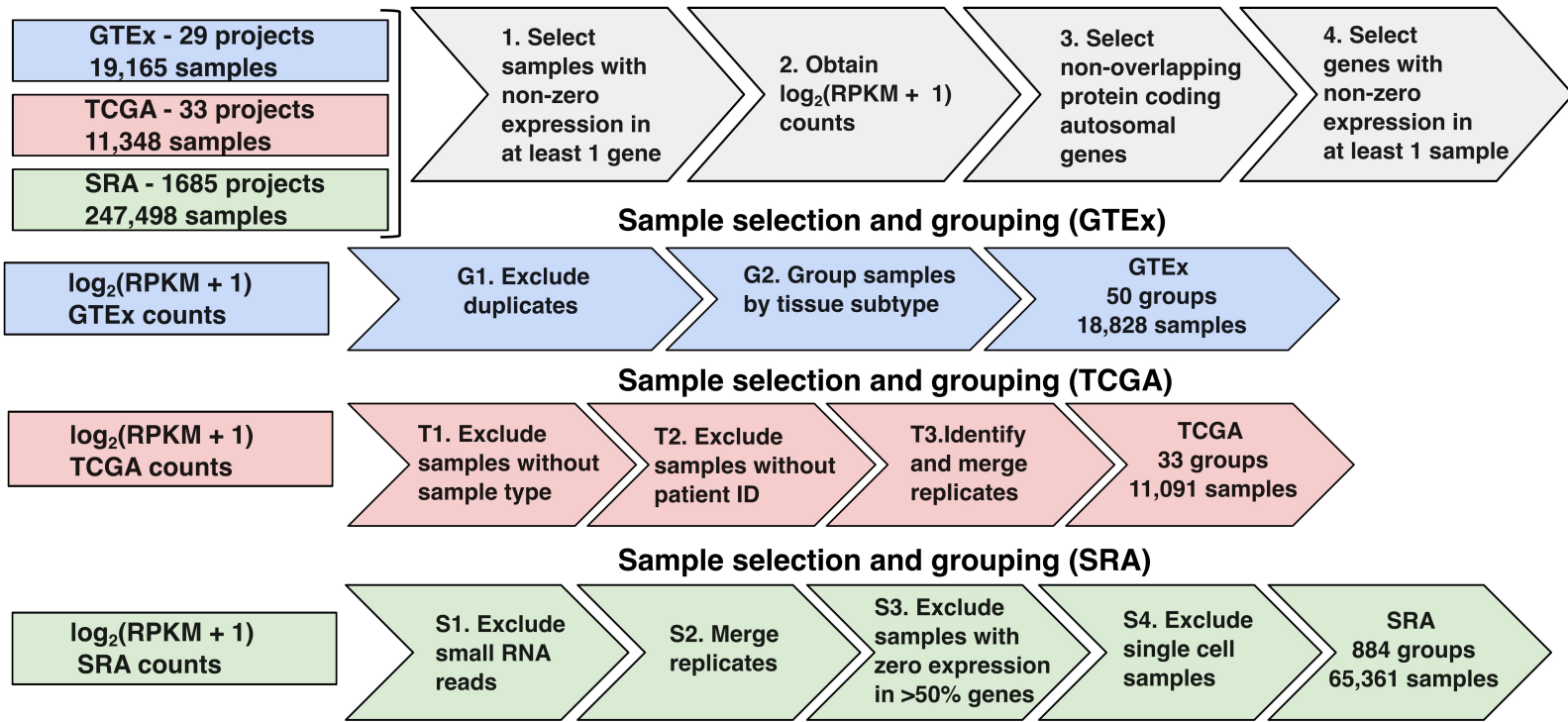
1208

1209 **Figure 4: Heritability enrichment of network annotations** Mean and standard deviation of  
 1210 heritability enrichment and the coefficient  $\tau^*$ , an estimate of the heritability of SNPs unique to  
 1211 the annotation. All genes: whether a variant was located in a 100 kilobase window of all  
 1212 protein-coding genes (Translucent), All genes + baseline: all-genes annotation in addition to 97  
 1213 functional annotations such as known enhancer and promoter regions (Opaque). **(A)**  
 1214 Meta-analysis of 42 independent traits for six centrality measures obtained from the universal  
 1215 consensus network and non-cancer consensus networks corresponding to values of the  
 1216 penalization parameter  $\lambda$  between 0.14 - 0.20. **(B)** Meta-analysis of 9 blood-related traits  
 1217 including, Crohn's disease, Ulcerative colitis, Rheumatoid arthritis, Allergy Eczema, Eosinophil  
 1218 count, Red blood cell count, White blood cell count, Red blood cell width, and Platelet count for  
 1219 network annotations from Blood GTEx ( $\lambda = 0.24 - 0.32$ ), Blood consensus ( $\lambda = 0.18 - 0.26$ ), and  
 1220 Universal consensus network ( $\lambda = 0.14 - 0.20$ ). **(C)** Meta-analysis of 9 CNS-related traits  
 1221 including, Alzheimer's disease, Epilepsy, Parkinson's disease, Bipolar disorder, Smoking  
 1222 cessation, Waist-hip-ratio adjusted BMI, Schizophrenia, Major depressive disorder, and Number  
 1223 of alcoholic drinks per week, for network annotations corresponding to 6 centrality measures  
 1224 derived from CNS GTEx ( $\lambda = 0.26 - 0.32$ ), CNS ( $\lambda = 0.20 - 0.28$ ), and Universal consensus  
 1225 network ( $\lambda = 0.14 - 0.20$ ).

1226

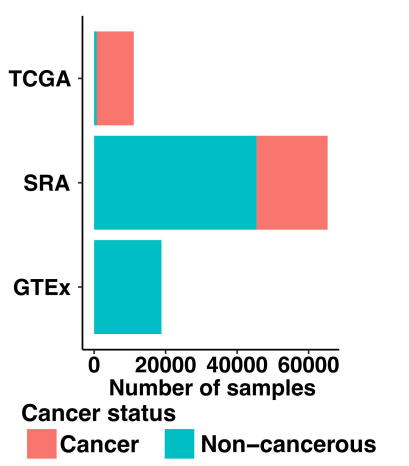
**A**

**Data normalization and log transformation**



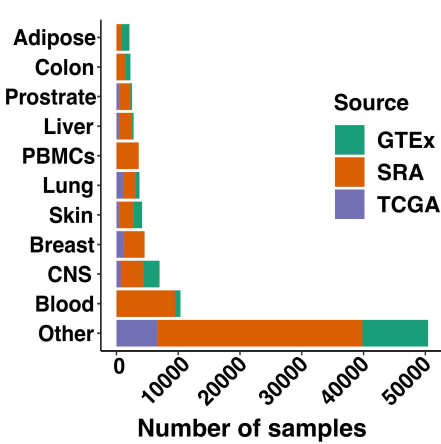
**B**

**Prevalence of Cancerous Samples in SRA, GTEX, and TCGA**



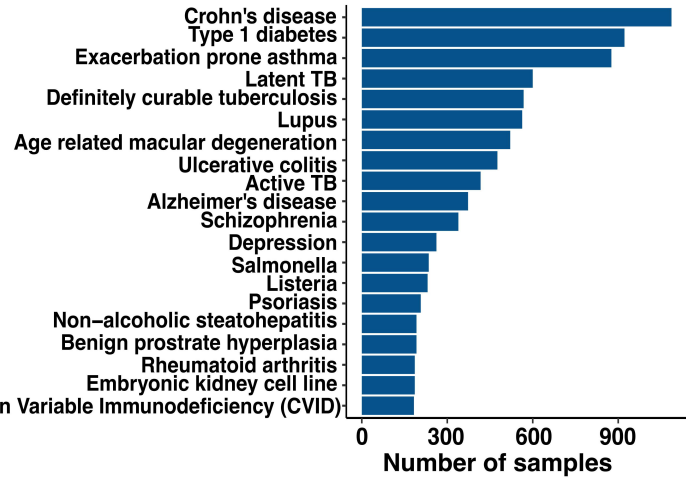
**C**

**Most prevalent tissues in SRA, GTEX, and TCGA**



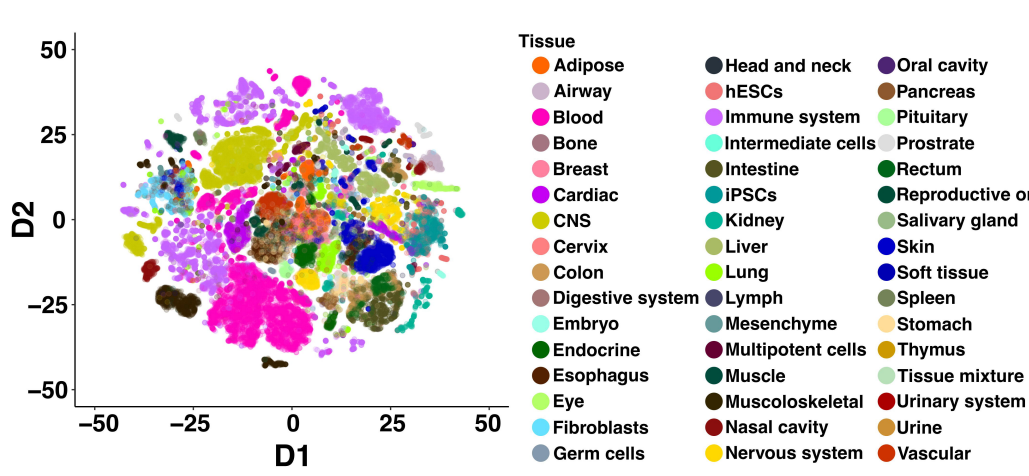
**D**

**Most prevalent diseases in SRA excluding cancer**



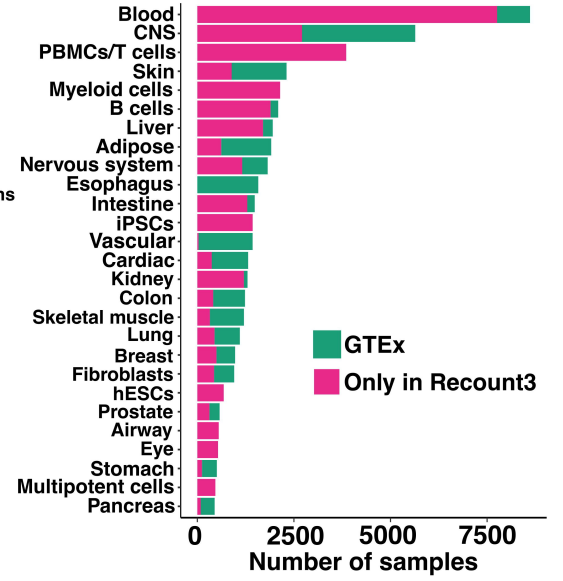
**E**

**t-SNE visualization of cell type enrichment scores of 63193 non-cancerous samples representing 48 tissue contexts**

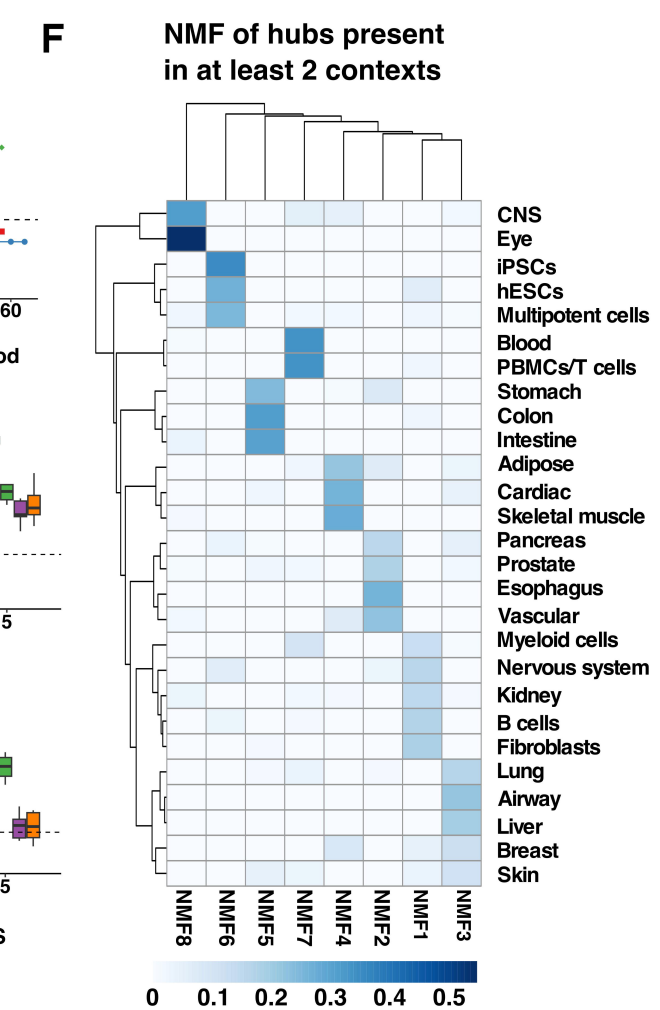
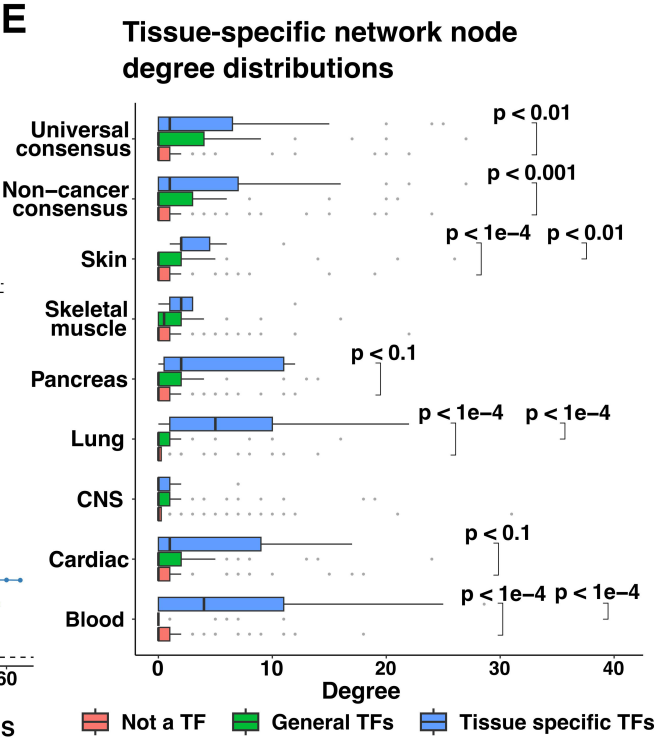
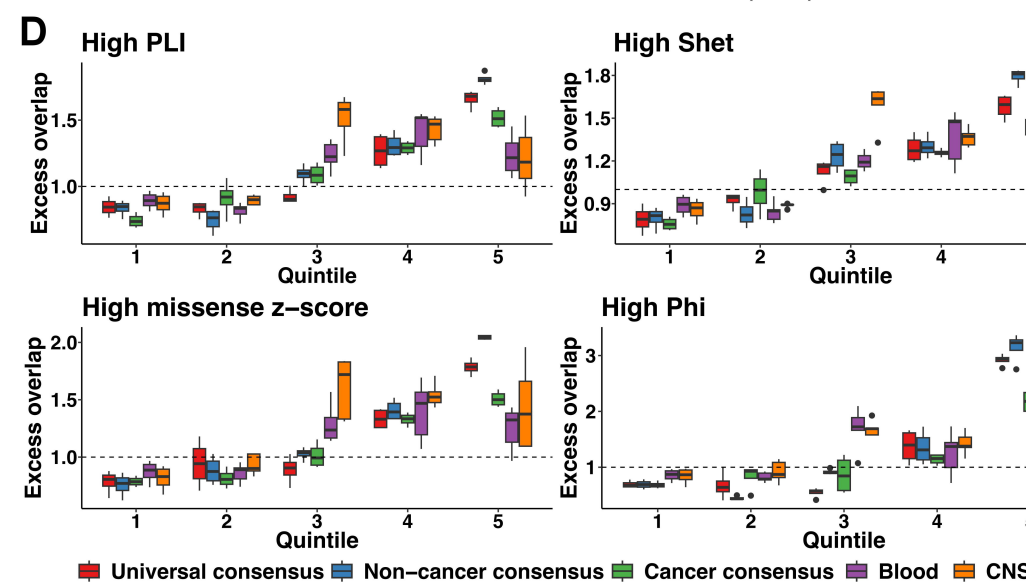
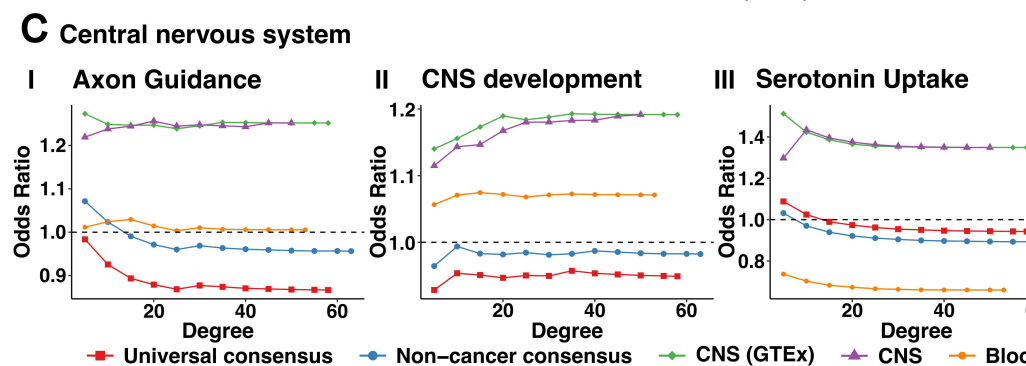
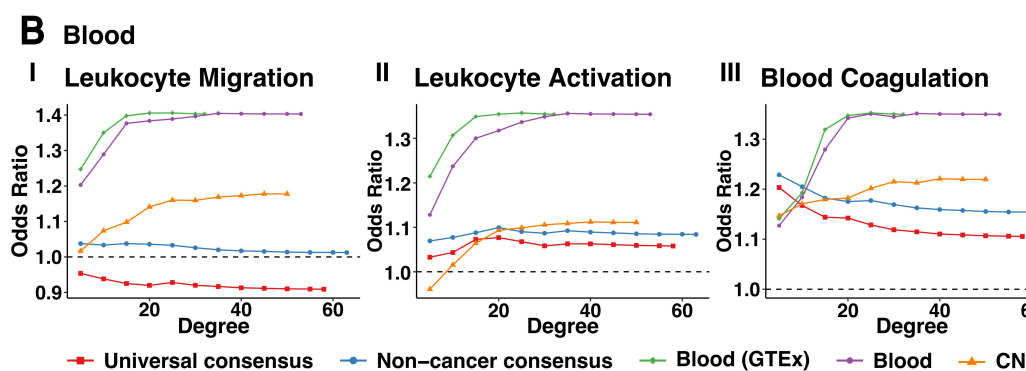
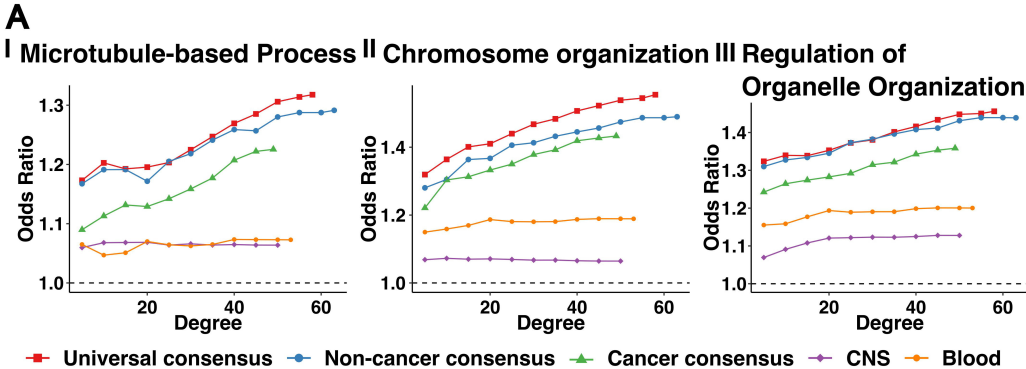


**F**

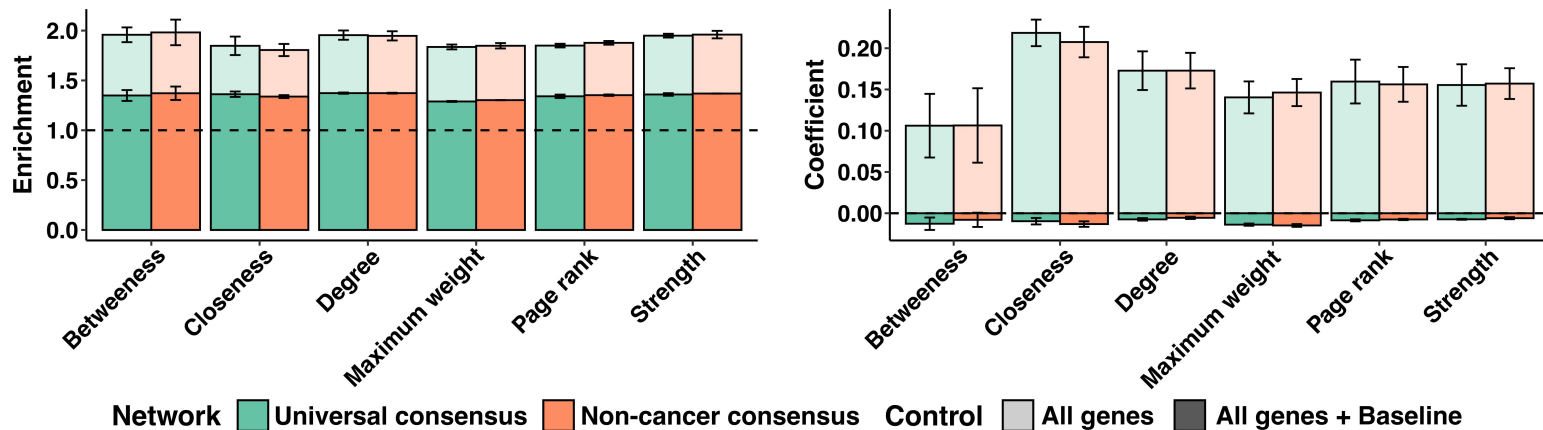
**Increase in sample size across 27 contexts with 500 or more samples**



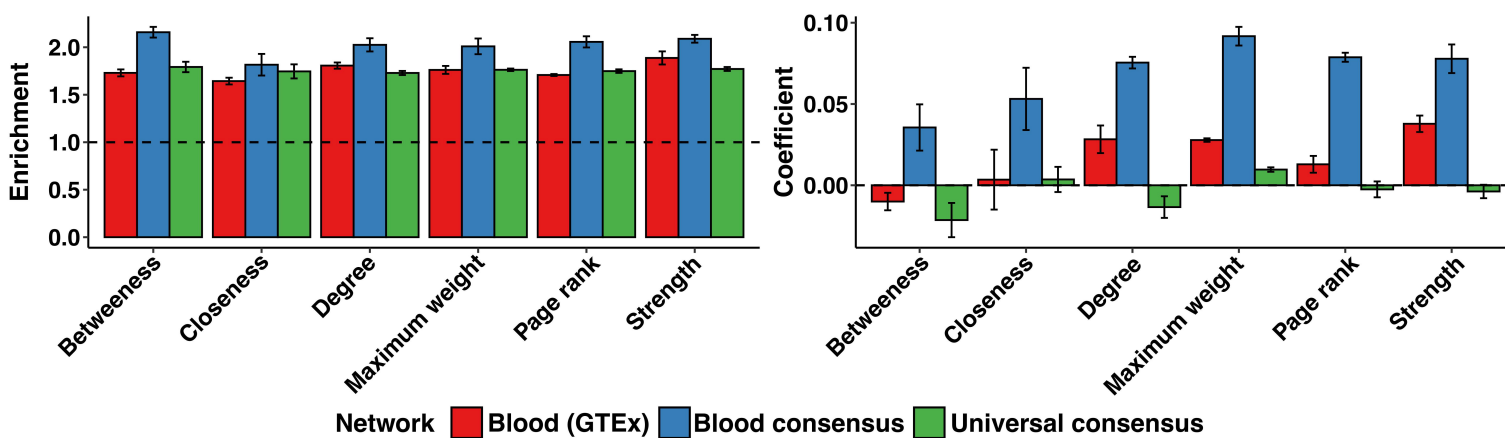




## A Meta-Analysis of 42 Independent Traits



## B Meta-Analysis of 9 Blood Related Traits (Conditioned on All genes and Baseline)



## C Meta-Analysis of 9 CNS Related Traits (Conditioned on All genes and Baseline)

